Research Paper

Tertiary lymphoid structure stratifies glioma into three distinct tumor subtypes

Xingwang Zhou[1], Wenyan Li[1], Jie Yang[1], Xiaolan Qi[2], Yimin Chen[1], Hua Yang[1], Liangzhao Chu[1]

[1]Department of Neurosurgery, The Affiliated Hospital of Guizhou Medical University, Guiyang 550004, Guizhou Province, PR China
[2]Key Laboratory of Endemic and Ethnic Diseases, Ministry of Education and Key Laboratory of Medical Molecular Biology of Guizhou Province, Guizhou Medical University, Guiyang 550004, Guizhou Province, PR China

Correspondence to: Liangzhao Chu; **email:** 365446506@qq.com, https://orcid.org/0000-0003-2289-7624
Keywords: tertiary lymphoid structure, glioma, TCGA, CGGA
Received: September 13, 2021 **Accepted:** December 11, 2021 **Published:** December 26, 2021

ABSTRACT

Objective: Tertiary lymphoid structure (TLS), also known as ectopic lymphoid organs, are found in cancer, chronic inflammation, and autoimmune diseases. However, the heterogeneity of TLS in gliomas is unclear. Therefore, it is necessary to identify TLS differences and define TLS subtypes.
Methods: The TLS gene profile of 697 gliomas from The Cancer Genome Atlas (TCGA) was used for consensus clustering to identify robust clusters, and the reproducibility of the stratification method was assessed in Chinese Glioma Genome Atlas (CGGA) cohort1, CGGA_cohort2, and GSE16011. Analyses of clinical characteristics, immune infiltration, and potential biological functions were performed for each subtype.
Results: Three resulting clusters (A, B, and C) were identified based on consensus clustering on the gene expression profile of TLS genes. There was a significant prognostic difference among the clusters, with a shorter survival for C than B and A. In comparison with the A and B subtypes, the C subtype was significantly enriched in primary immunodeficiency, intestinal immune network for IgG production, antigen processing and presentation, natural killer cell-mediated cytotoxicity, complement and coagulation cascades, cytokine-cytokine receptor interaction, leukocyte transendothelial migration, and some immune-related diseases. The levels of 23 immune cell types were higher in the C subtype than in the A and B subtypes. Finally, we developed and validated a riskscore based on TLS subtypes with better performance of prognosis prediction.
Conclusions: This study presents a new stratification method according to the TLS gene profile and highlights TLS heterogeneity in gliomas.

INTRODUCTION

Gliomas are common malignant tumors in the central nervous system [1]. Although glioma patients receive tumor resection following chemotherapy and radiotherapy [2], as well as tumor-treating fields [3], their prognosis remains poor. As a result, understanding the biological mechanism of glioma progression is crucial for glioma therapy. Immunotherapy, which is used to modulate lymphocytes to attack tumor cells and prevent tumor progression, has attracted considerable attention [4]. However, the efficacy of immunotherapy for glioblastoma patients is limited [5]. Therefore, it is important to further analyze potential resistance factors and develop new treatment strategies.

Tertiary lymphoid structure (TLS), also known as ectopic lymphoid organs, are found in cancer, chronic inflammation, and autoimmune diseases [6]. The composition in cancer-associated TLSs includes B cells, follicular dendritic cells (FDCs), plasma cells, T cells, neutrophils, macrophages, and high endothelial venules

(HEVs) [6]. B cell follicles with germinal center characteristics and a T cell-rich zone with mature dendritic cells (DCs) are surrounded by plasma cells. HEVs are found in the vicinity of TLSs, which can mediate the entry of lymphocytes into TLSs [7]. The presence of TLSs has been reported in various tumors including head and neck squamous cell carcinoma [8], lung cancer [9], sarcomas [10], and even gliomas [11]. Furthermore, the presence of TLS has been found to be associated with a good prognosis in the majority of cancers [8–10, 12, 13] and improve the effectiveness of immunotherapy, indicating that TLSs may generate anti-tumorigenic immune cells, which play a vital role in the immune response against tumors. However, some studies indicated that TLS presence may lead to tumor progression, which may be associated with microniches for cancer progenitor cells. Thus far, only one study has evaluated the distribution of TLSs in gliomas [11], and the results showed that αCD40 enhanced the formation of TLSs via the stimulation of B cells while reducing CD8+ T cell cytotoxicity in the brain of glioma-bearing mice [11]. Therefore, it is crucial to determine the TLS profile and identify TLS subtypes in gliomas, which may contribute to the development of new treatment methods.

In the present study, we stratified gliomas into three subtypes according to the unsupervised clustering of TLS signature expression profiles. Three independent cohorts were used to verify the reproducibility and stability of this classification method. Each of the three TLS subtypes had distinct clinical characteristics, biological functions, and immune infiltration patterns. Our findings shed light on TLS heterogeneity in gliomas, and the clinical stratification of TLS may contribute to the development of TLS-targeted therapy.

RESULTS

Differential expression and survival analysis

The locations of CNVs and CNV frequency in TLS genes were determined (Figure 1A and 1C). Among 896 glioma patients, only 36 (4.02%) patients harbored somatic mutations in TLS genes (Figure 1B). We evaluated the gene expression profile of TLS genes in glioma and normal tissues (TCGA vs. GTEx). We found that the expression levels of CXCL2, CCL3, CCL4, CCL5, CCL8, CCL18, CXCL9, CXCL8, CXCL11, CXCL13, CD4, CCR5, CXCR3, CSF2, IGSF6, IL2RA, CD38, CD5, SDC1, GFI1, IL1R1, IL10, CCL20, IRF4, TRAF6, STAT5A, ICOS, SH2D1A, TIGIT, PDCD1 were higher in glioma tissues than in normal tissues (Figure 1D, $p < 0.001$); however, CXCL19, CXCL21, TNFRSF17, IL1R2, MS4A1, CD40, SGPP2, CD200, and FBLN7 were downregulated in glioma tissues ($p < 0.001$). Survival analysis indicated that 36 of these 40 genes were associated with the prognosis of glioma in the TCGA cohort (Figure 2A, $p < 0.05$), the genes associated with the prognosis of glioma were identified in CGGA_cohort1, CGGA_cohort2, and GSE16011 (Figure 2B–2D).

Identification of three subtypes in gliomas with consensus clustering

To characterize TLS heterogeneity in gliomas, the 40 TLS genes were used to perform clustering analysis (Supplementary Figure 1). Three clusters (A, B, and C) were identified based on consensus clustering on the gene expression profile of TLS genes (Figure 3A). PCA was carried out to confirm the assignments of subtypes and validate the differences in expression characteristics among the three TLS subtypes (Figure 3B). There was a significant prognostic difference among the clusters, with a shorter survival for C than B and A (Figure 3C, $p < 0.001$).

CGGA_cohort1, CGGA_cohort2, and GSE16011 were used to verify the reproducibility and stability of this classification method in the TCGA cohort (Figure 4). The results showed high consistency between the subtypes of the TCGA cohort and CGGA_cohort1, CGGA_cohort2, and GSE16011 (Supplementary Table 1). In addition, the TLS subtypes of the testing cohorts showed a similar pattern of expression and prognostic characteristics to the TCGA cohort (Figure 4).

Relationship between TLS subtypes and clinical features

We evaluated the clinical relevance of the identified TLS subtypes. The results indicated that WHO grade III, WHO grade IV, IDH wild-type, 1p19q non-codeletion, glioblastoma, and anaplastic glioma were associated with the C subtype (Figure 3). However, the A subtype was associated with WHO grade II, IDH mutation, 1p19q codeletion, astrocytoma, oligodendroglioma, and oligodendroastrocytoma (Figure 3 and Supplementary Table 2). Similarly, the relationship of TLS subtypes with clinicopathological characteristics was observed in CGGA_cohort1, CGGA_cohort2, and GSE16011 (Figure 4, Supplementary Tables 3–5). Furthermore, we also observed that most classical, neural, proneural gliomas were A subtype, while most mesenchymal gliomas was C subtype (Supplementary Tables 2 and 4).

Potential biological functions related to TLS subtypes

GSEA was used to identify potential biological functions related to the TLS subtypes. In comparison

with the A and B subtypes, the C subtype was significantly enriched in primary immunodeficiency, intestinal immune network for lgG production, antigen processing and presentation, natural killer cell-mediated cytotoxicity, complement, and coagulation cascades, cytokine-cytokine receptor interaction, leukocyte transendothelial migration, and some immune-related diseases such as asthma and systemic lupus erythematosus (Supplementary Figures 2 and 3). In comparison with the A subtype, the B subtype was significantly enriched in cytokine-cytokine receptor interaction, natural killer cell-mediated cytotoxicity, primary immunodeficiency, intestinal immune network for lgG production, antigen processing and presentation, and some immune-related diseases such as asthma and systemic lupus erythematosus (Supplementary Figure 4). Similar results were obtained for CGGA_cohort1, CGGA_cohort2, and GSE16011 (Supplementary Figures 5–13).

Immune infiltration of TLS subtypes in gliomas

We used ssGSEA to determine the functions and enrichment levels of immune cells. The levels of 23 immune cell types were higher in the C subtype than in the A and B subtypes, such as activated B cells, activated CD4 T cells, activated CD8 T cells, and activated DCs (Figure 5A and 5B). In terms of immune function, APC co-inhibition, APC co-stimulation, CCR, immune checkpoint, cytolytic activity, HLA, inflammation promotion, MHC class I, parainflammation, type I IFN response, and type II IFN response were significantly enriched in the C subtype compared with the A and B subtypes (Figure 5B and 5C). In addition, we found that the C subtype had higher immune, stromal, and ESTIMATE scores compared with the scores of the A and B subtypes (Figure 5D and 5E); however, tumor purity was lower (Figure 5F). To validate the results, we quantified the immune

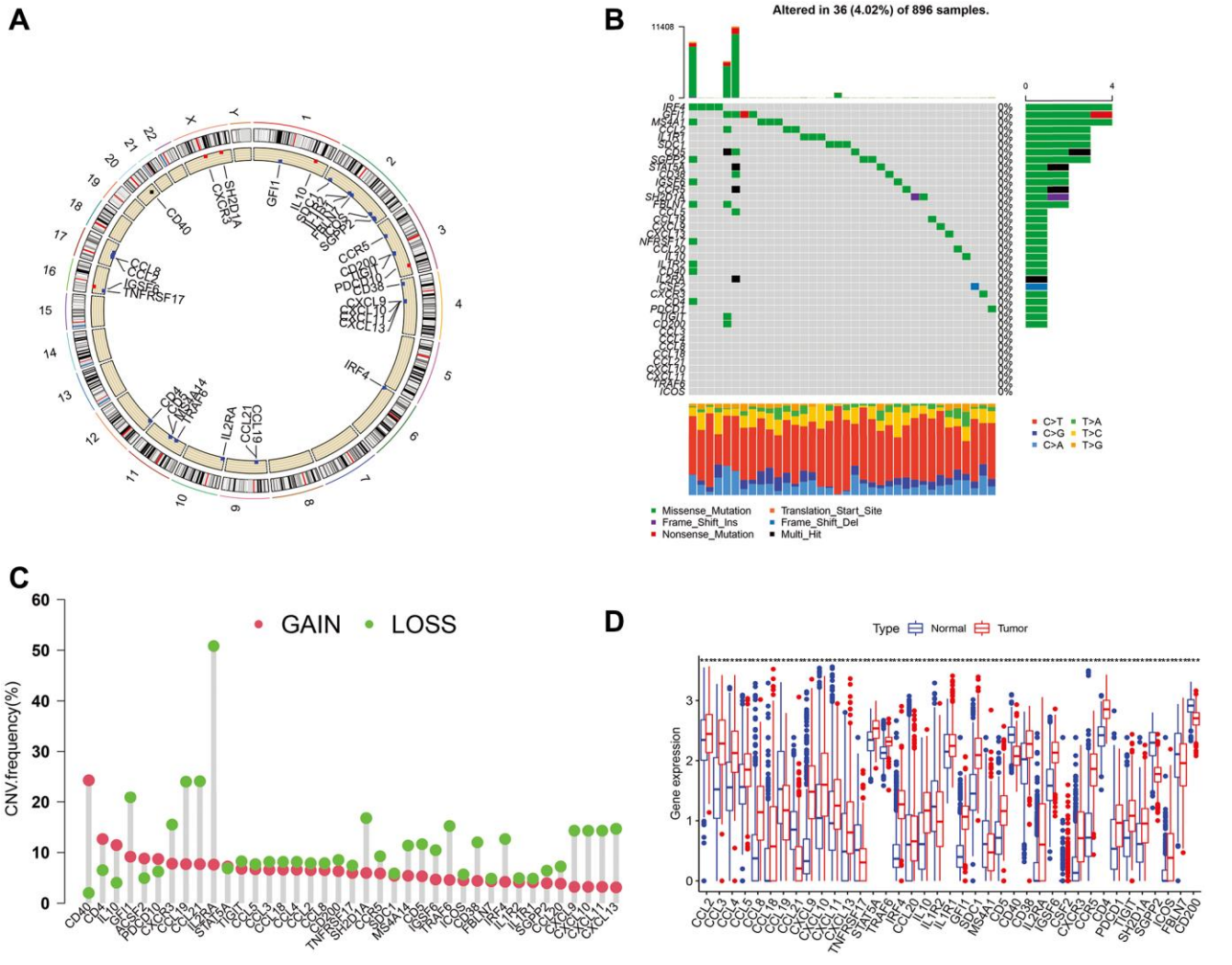

Figure 1. Mutations, CNVs, and diffent expresion of TLS genes in TCGA cohort. (**A**) The location of CNVs of TLS genes on 23 chromosomes. (**B**) The somatic mutation frequency of TLS genes in TCGA cohort. (**C**) The CNV frequency of TLS genes. (**D**) The different expresion of TLS between 697 gliomas and 1157 normal brain tissues.

infiltration, immune, stromal, and ESTIMATE scores of each subtype in GSE16011, CGGA_cohort1, and CGGA_cohort2, and consistent results were obtained (Supplementary Figures 14–17).

The potential therapeutic value of TLS subtype

To further understand the effect of the TLS subtype on the drug response, we evaluate the relationship between distinct TLS subtypes and drug sensitivity. We found that drug sensitivity associated with C subtype, including AG.014699, BAY.61.360, BIRB.0796, BMS.754807, CCT007093, EHT.1864, Elesclomol, FH535, GW.441756, Imatinib, Lenalidomide, LFM.A13, OSI.906, PD.173074, PD.0332991, PF.562271, QS11, Thapsigargin, Vinorelbine, Vorinostat, VX.702, ABT.263, AICAR, AZD.0530, AZD8055, BMS.708163, Gefitinib (Supplementary Table 6). The drug sensitivity correlated with B subtype including AP.24534, AS601245, ATRA, and so on. However, many drugs showed a high sensitivity for the A subtype, such as Parthenolide, Paclitaxel, and Temsirolimus (Figure 6 and Supplementary Table 6). All in all, these results indicate that TLS correlated with drug sensitivity. Thus, the TLS may be a potential biomarker for establishing appropriate treatment strategies.

Calculation of riskscores and validation

To further analyze the characteristics of the three subtypes, genes with differential expression within subtypes were enquired with the R package "samr". There were 5151 intersection genes between the A and B subtypes, A and C subtypes, and B and C subtypes in the TCGA cohort (Figure 7A). The intersection genes between subtypes in CGGA_cohort1 (Figure 7B), CGGA_cohort2 (Figure 7C), and GSE16011

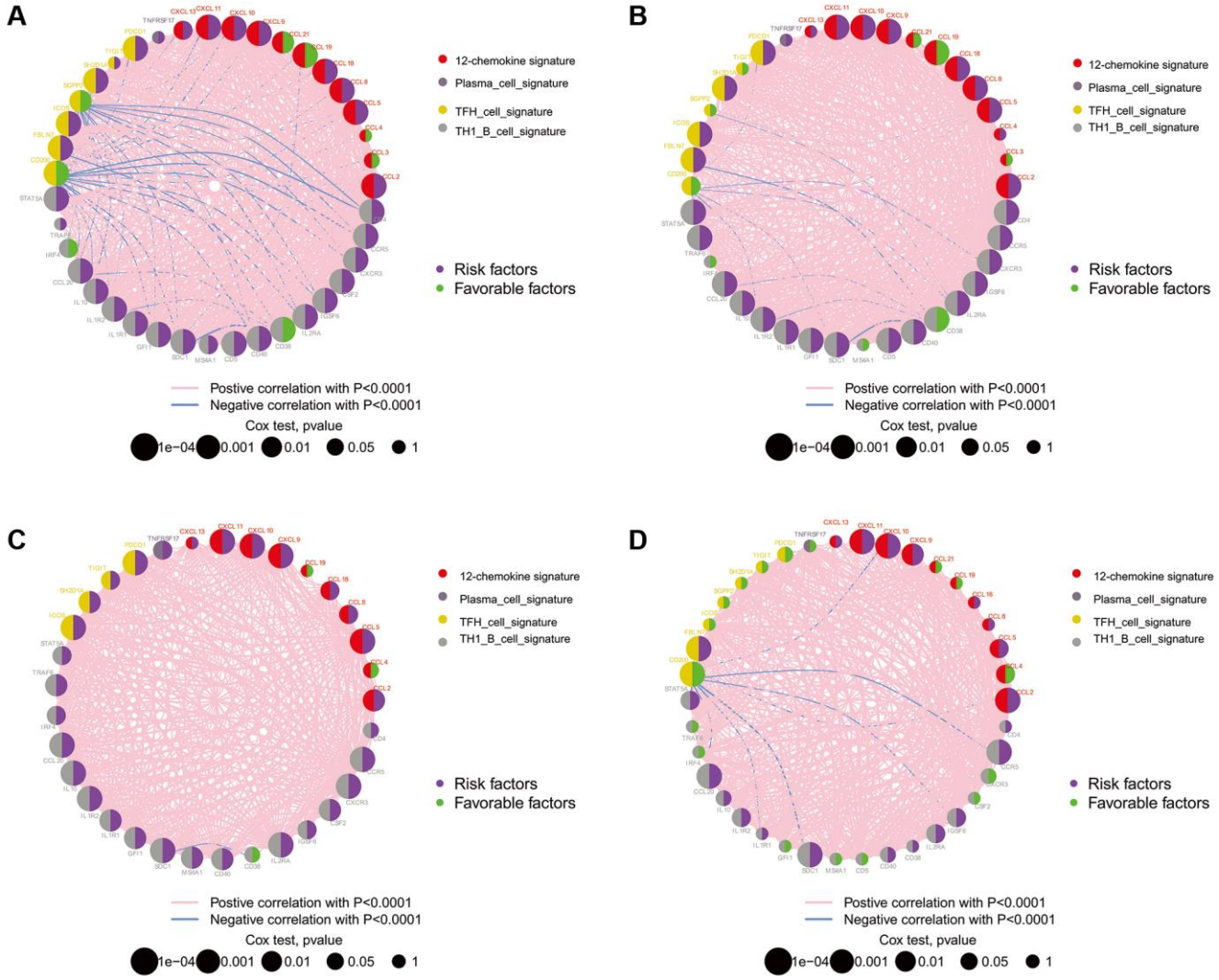

Figure 2. The prognostic effect of TLS genes in glioma of TCGA, CGGA and GSE16011. (**A**) TCGA; (**B**) CGGA_cohort1; (**C**) CGGA_cohort2; (**D**) GSE16011. All of the TLS genes were associated with prognosis of glioma patients in these four datasets.

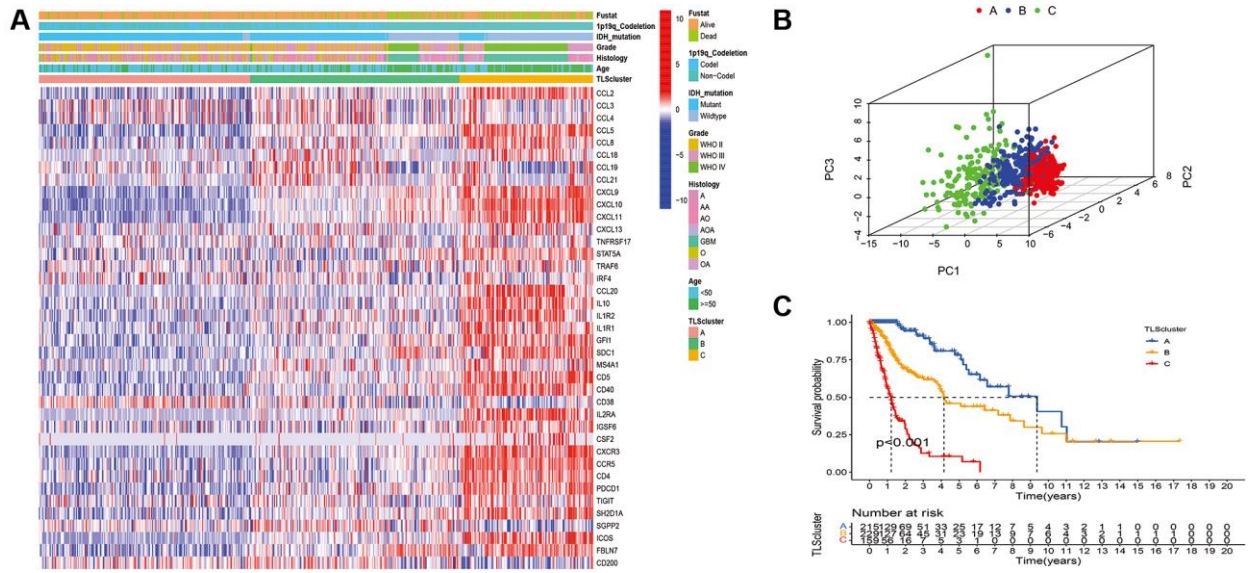

Figure 3. Identification of distinct TLS subtypes in glioma through TLS gene profiling. (**A**) Heatmaps of three TLS subtypes defined in TCGA cohorts and the relation between TLS subtypes and clinical features. (**B**) Principal component analysis (PCA) of three metabolic subtypes using candidate genes. (**C**) Survival analyses show significant differences between the three TLS subtypes in TCGA cohorts.

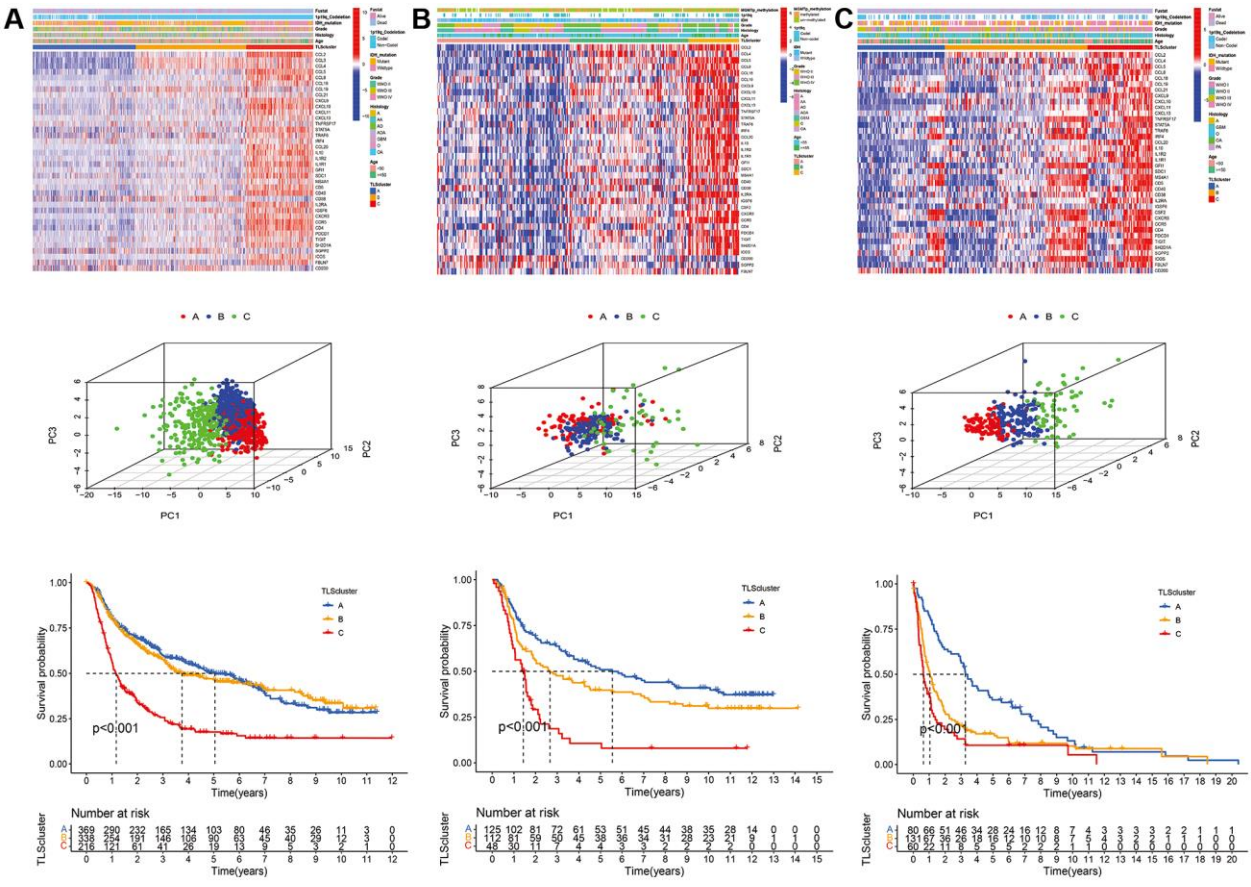

Figure 4. Validation of TLS subtypes in CGGA_cohort1, CGGA_cohort2 and GSE16011. (**A**) Heatmap of three TLS subtypes defined in CGGA_cohort1 cohorts and the relation between TLS subtypes and clinical features, PCA of three metabolic subtypes using candidate genes, survival analyses show significant differences between the three TLS subtypes in CGGA_cohort1. (**B**) heatmaps, PCA and survival analyses in CGGA_cohort2. (**C**) heatmaps, PCA and survival analyses in GSE16011.

(Figure 7D) were identified. The intersection genes from TCGA, CGGA_cohort1, CGGA_cohort2, and GSE16011 were then analyzed again using the R package "Venn" (Figure 7E). Finally, a total of 296 genes were identified. Among these genes, only 44 genes were differentially expressed (24 downregulated and 20 upregulated) between glioma and normal tissues (Figure 7F and 7G). Of the 44 genes, 28 genes were associated with prognosis and selected for LASSO regression analysis to identify the best genes for calculating riskscores in the TCGA dataset. Finally, 14 genes (HAMP, CARD16, TRIM38, CCR5, S100A8, MSR1, S100A9, S100A4, CHI3L2, PLAU, GCH1, P2RY8, UPP1, PROS1) were obtained, and riskscores were calculated with regression coefficients. Survival analysis indicated that patients with high riskscores had shorter overall survival compared with that of patients with low riskscores (Figure 8A). Moreover, multivariate Cox regression analysis suggested that the riskscore was an independent factor in predicting the prognosis of gliomas (Supplementary Figure 17). Analysis of clinical relevance revealed that a high riskscore was related to gliomas with WHO grade IV or IDH wild-type (Figure 8B). The AUCs of riskscores in predicting the 1-year, 3-year, and 5-year survival were 0.877, 0.904, and 0.897, respectively (Figure 8C). We validated this TLS signature in CGGA_cohort1, CGGA_cohort2 and GSE16011, and consistent results were obtained (Figure 8D–8L).

The clinical significance of intersection proteins between subtypes in glioma confirmed by immunohistochemistry

We used immunohistochemistry to evaluate the expression of the above-mentioned 14 genes (HAMP, CARD16, TRIM38, CCR5, S100A8, MSR1, S100A9, S100A4, CHI3L2, PLAU, GCH1, P2RY8, UPP1, PROS1) in glioma and normal tissues. The results showed that TRIM38, CCR5, PLAU, P2RY8, and PROS1 have a higher immunoreaction score (IRS) in tumors than normal tissues ($p < 0.05$, Figure 9A–9C),

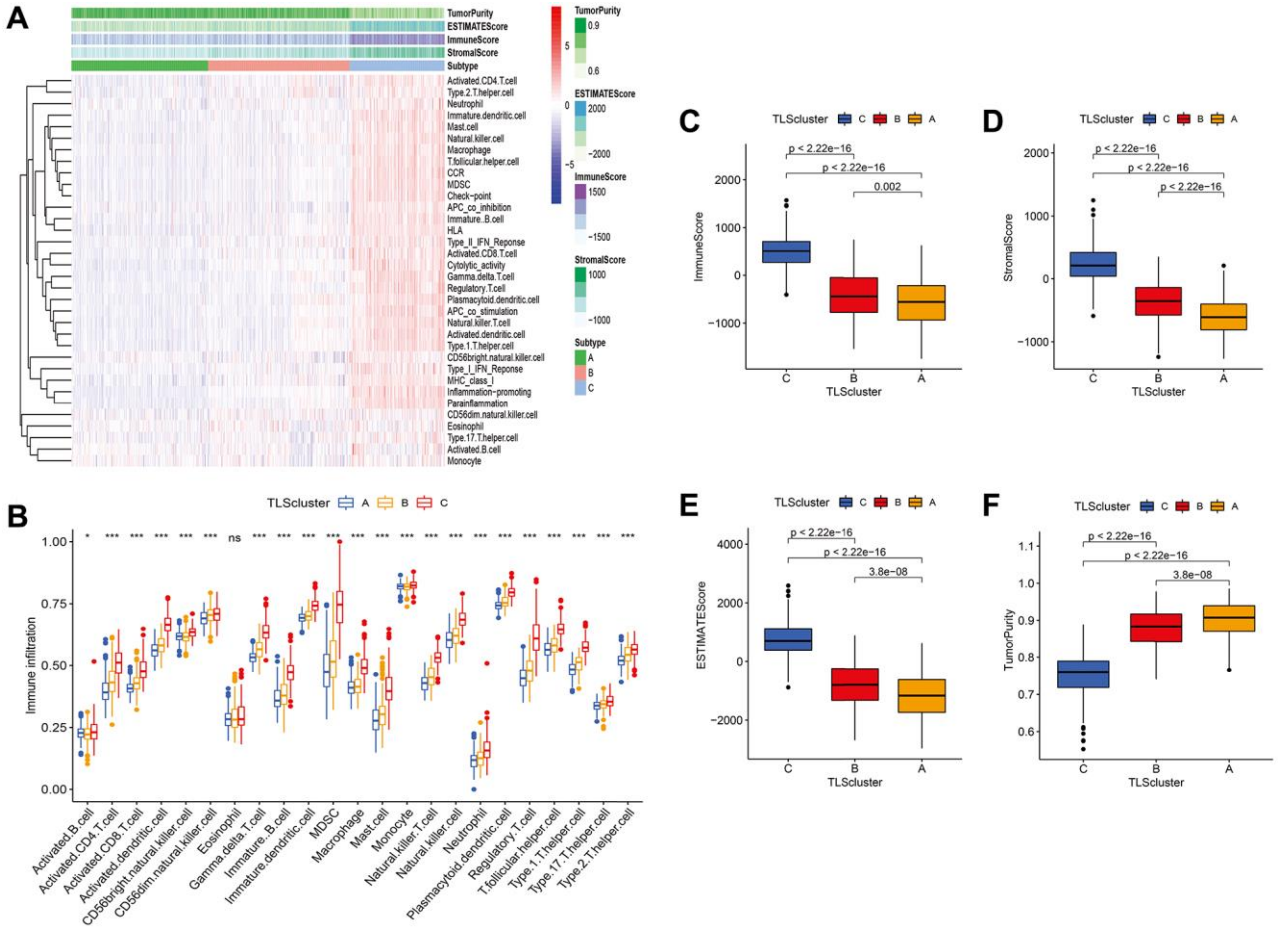

Figure 5. Immune infiltration and tumor microenvironment of three TLS subtypes in TCGA cohort. (**A**) Heatmap of TLS subtypes associated with immune infiltration and immune funtion. (**B**) the signature of 23 immune cell among TLS subtypes. (**C**–**F**) tumor microenvironment of TLS subtypes. (**C**) subtype had higher immune, stromal, and ESTIMATE scores compared with the scores of the A and B subtypes; however, tumor purity was lower (Figure 5C–5F).

while the IRS of HAMP and S100A9 in gliomas were lower than normal tissues ($p < 0.05$, Figure 9A–9C). No significant differences were observed for the expression of the remaining proteins between tumor and normal tissues. Furthermore, we assess the differential expression of the 14 proteins between high and low-grade gliomas. We observed that the IRSs of PROS1, P2RY8, PLAU, CHI3L2, MSR1, CCR5, and TRIM38 were higher than its corresponding IRSs in low-grade glioma, while the IRSs of HAMP, CARD16, and S100A8 in high-grade glioma were lower than low-grade glioma (Figure 9D). However, no one of those 14 proteins were found to be associated with IDH1 mutation (Figure 9E).

DISCUSSION

Gliomas are one of the most common primary tumors in adult patients, which can lead to high mortality and morbidity due to rapid progression and treatment resistance. TLSs are discrete, structured organizations of infiltrating immune cells, which have been found to improve immunotherapy and survival in several cancers. In the present study, we stratified gliomas into three subtypes according to the unsupervised clustering of TLS signature expression profiles. The relevance of clinical characteristics, immune infiltration, tumor microenvironment, potential biological functions was investigated. The findings may shed light on the

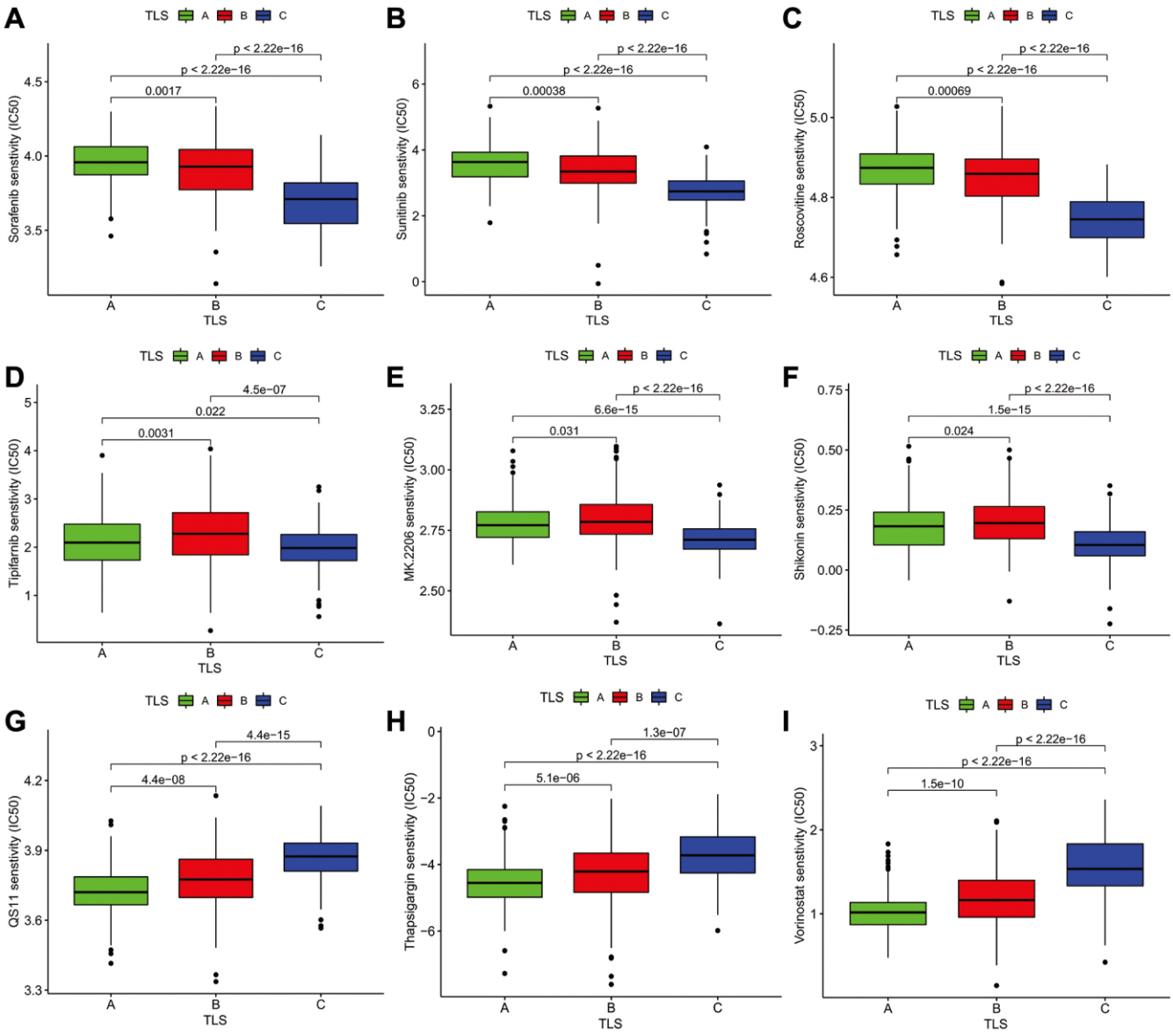

Figure 6. The Association analysis of TLS subtype and drug sensitivity. (**A–C**) Sorafenib, Sunitinib, Roscovitine were the most sensitive drugs to A subtype. (**D–F**) Tipifarnib, MK.2206, and Shikonin were the most sensitive drugs to B subtype. (**G–I**) QS11, Thapsigargin, and Vorinostat were the most sensitive drugs to C subtype.

molecular subtypes of gliomas and deepen our understanding of TLS heterogeneity in gliomas.

An increasing number of studies have shown that an orchestrated immune response to cancer is elicited locally in TLS, which resemble the structures of secondary lymphoid organs [14]. TLS predominantly consists of B cells and T cells. FDCs and germinal centers (GCs) can be used to determine the maturation of TLS. FDCs but not GCs are enriched in B cells and T cells in the intermediate mature stage; however, both FDCs and GCs are found in mature TLSs. Neither FDCs nor GCs is found in immature TLS [15, 16]. Together with T and B cells, DCs, neutrophils, macrophages, HEVs, CD4+ T follicular helper cells (T_{FH}), CD8+ cytotoxic T cells, CD4+ regulatory T cells (T_{Reg}), and innate lymphoid cells can be detected in TLS [14]. Several gene signatures have been used to detect TLSs in the transcriptomic analyses of human cancers, which include 12 chemokine signatures, T_{FH} cell signatures, T_H1 and B cell signatures, and plasma cell signatures [6]. To ensure the successful detection of all TLS, these gene signatures were used to investigate TLS heterogeneity in gliomas. The prognostic role of TLSs has been reported in various cancers. The presence of TLS detected by immunohistochemistry was associated with favorable clinical outcomes for lung metastases in colorectal cancer, liver metastases in colorectal cancer, lung cancer, and metastases in ovarian cancer [8–10, 12, 17]. In addition, some studies based on the 12 chemokine signatures indicated that TLSs may be associated with improved survival prognosis in hepatocellular carcinoma [18] and metastases of melanoma [19]. In the current study, 31 TLS genes were upregulated, whereas the other 9 genes were downregulated, and all of these genes were associated with glioma prognosis. Consistently, a significant survival difference was noted among the subtypes, with a shorter overall survival for the C subtype than the A and B subtypes. These results highlighted the importance of TLS-related genes and TLS heterogeneity in predicting the prognosis of glioma patients.

We investigated the association of TLS subtypes with clinical features in the TCGA cohort and found that malignant characteristics were enriched in the C subtype. However, the A subtype was associated with WHO grade II, IDH mutation, 1p19q codeletion, astrocytoma, oligodendroglioma, and oligodendroastrocytoma. Similarly, the relationship of TLS subtypes with clinicopathological characteristics

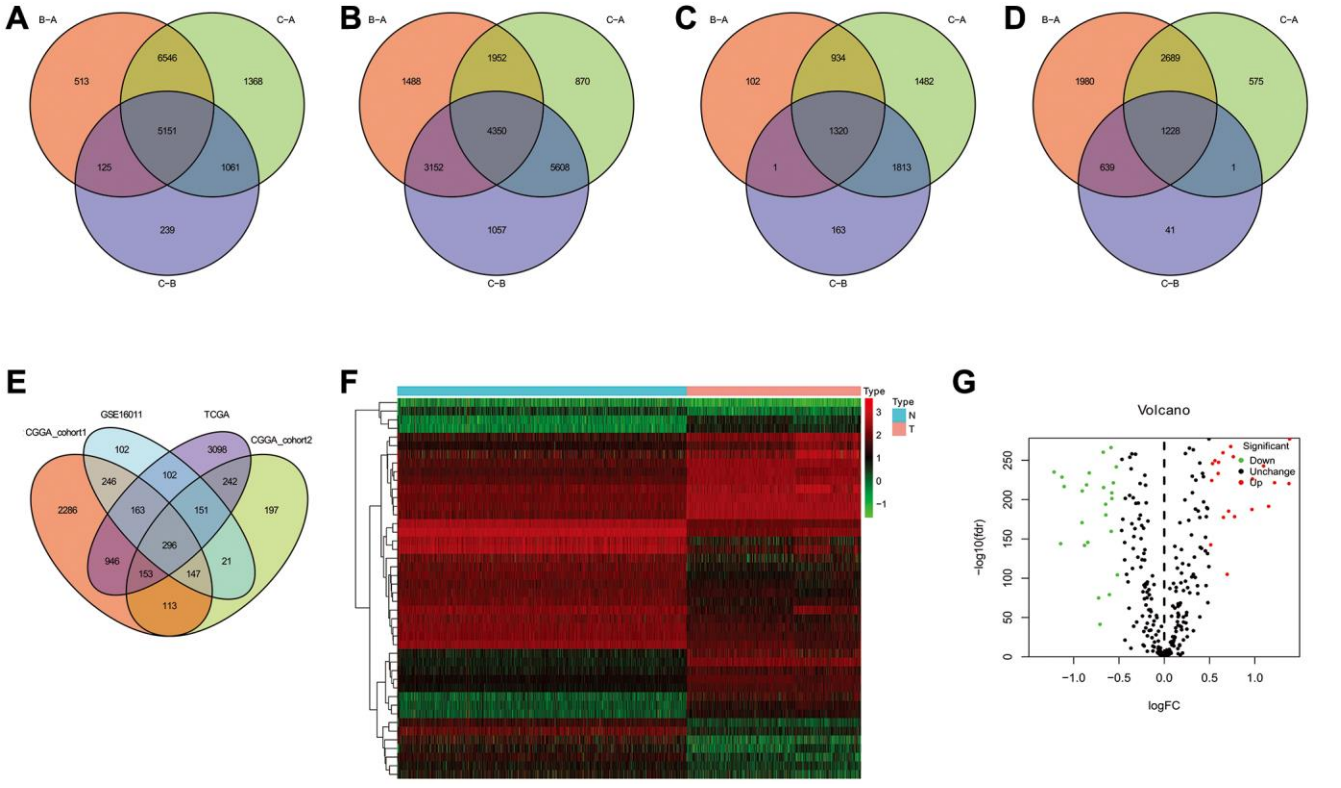

Figure 7. The common genes among TLS subtypes from TCGA, CGGA_cohort1, CGGA_cohort2 and GSE16011. (**A**–**D**) the intersection genes of TLS subtypes observed from TCGA, CGGA_cohort1, CGGA_cohort2 and GSE16011, respectively. (**E**) the common genes among TCGA, CGGA_cohort1, CGGA_cohort2 and GSE16011. (**F**) the heatmap of different expresion of intersection genes between glioma and normal tissues. (**G**) volcanic map showed the up- and down-regulated common genes.

was observed in CGGA_cohort1, CGGA_cohort2, and GSE16011. Our findings could contribute to a better understanding of the pathology and molecular subtypes of gliomas.

TLSs have been reported to improve the immunotherapy of cancer patients, as they are the primary sites of the initiation and maintenance of the local immune response [20, 21]. The underlying mechanisms may involve the activation and differentiation of B cells into antibody-producing cells, which is consistent with the idea that TLSs could improve the *in situ* production of tumor-specific antibodies to enhance anti-tumor immunity [22, 23]. Furthermore, TLSs may increase the proportions of CD69+ and CD38+ activated T cells and CD8+ T cells with an effector memory phenotype, characterized by the overexpression of a set of genes characteristic of T_H1 cell skewing, T cell cytotoxicity, T cell activation, and T cell chemotaxis [7, 17, 24–27]. In this study, we

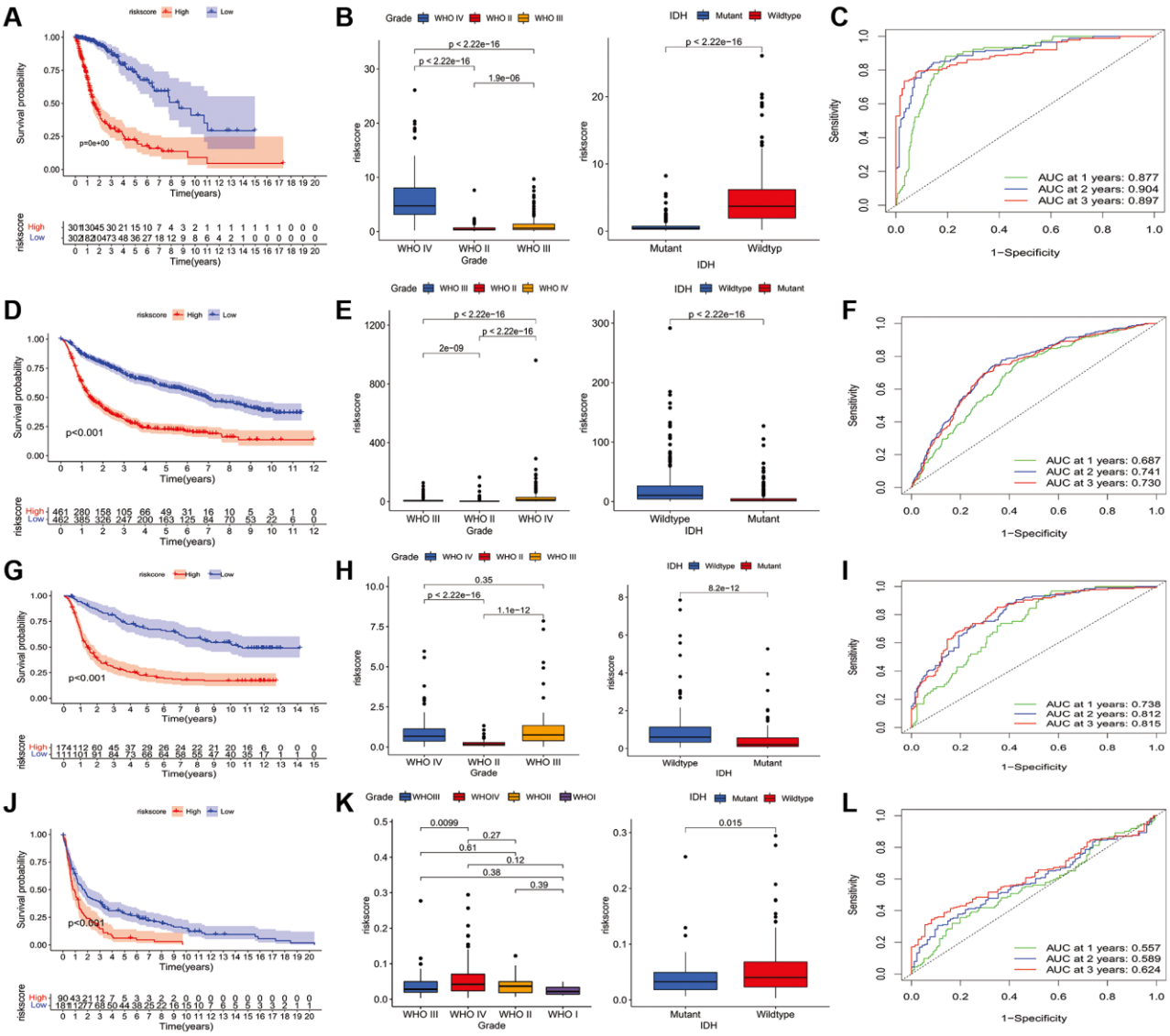

Figure 8. Construction of riskscore in TCGA and validation in CGGA and GSE16011 dataset. (**A**) The prognostic role of riskscore in TCGA glioma. (**B**) The relationship between riskscore and tumor grade, and IDH mutation status in TCGA database. (**C**) receiver operating characteristic curve indicated the survival prediction of riskscore in TCGA database; (**D**) The prognostic role of riskscore in glioma of CGGA1. (**E**) The relationship between riskscore and tumor grade, and IDH mutation status of CGGA1 cohort. (**F**) receiver operating characteristic curve indicated the survival prediction of riskscore in CGGA1 database. (**G**) The prognostic role of riskscore in glioma of CGGA2. (**H**) The relationship between riskscore and tumor grade, and IDH mutation status of CGGA2 cohort. (**I**) receiver operating characteristic curve indicated the survival prediction of riskscore in CGGA2 database. (**J**) The prognostic role of riskscore in glioma of GSE16011. (**K**) The relationship between riskscore and tumor grade, and IDH mutation status of GSE16011 cohort. (**L**) receiver operating characteristic curve indicated the survival prediction of riskscore in GSE16011 database. TCGA cohort was used as a discovery set, two CGGA cohorts and GSE16011 were employed as validation sets.

also found that the B and C subtypes were significantly enriched in primary immunodeficiency, intestinal immune network for lgG production, antigen processing and presentation, natural killer cell-mediated cytotoxicity, complement, and coagulation cascades, cytokine-cytokine receptor interaction, and leukocyte transendothelial migration. The C subtype have higher immune, stromal, and ESTIMATE scores compared with the scores of the A and B subtypes; however, tumor purity was lower. The levels of all 23 immune cell types were higher in the C subtype than in the A and B subtypes. These results demonstrated that the C subtype was a type of glioma with high immune infiltration but poor prognosis. Anti-tumorigenic immune cells such as natural killer cells, B cells, and CD8+ T cells were increased in C subtype, while pro-tumorigenic immune cells including M2 polarized macrophages, T-helper 2 cells, myeloid-derived suppressor cells, and regulatory T cells also increased, the beneficial effect of TLS may be reduced in patients. Previous studies indicated that immunosuppressive cells were presented in TLS such as regulatory T cells.

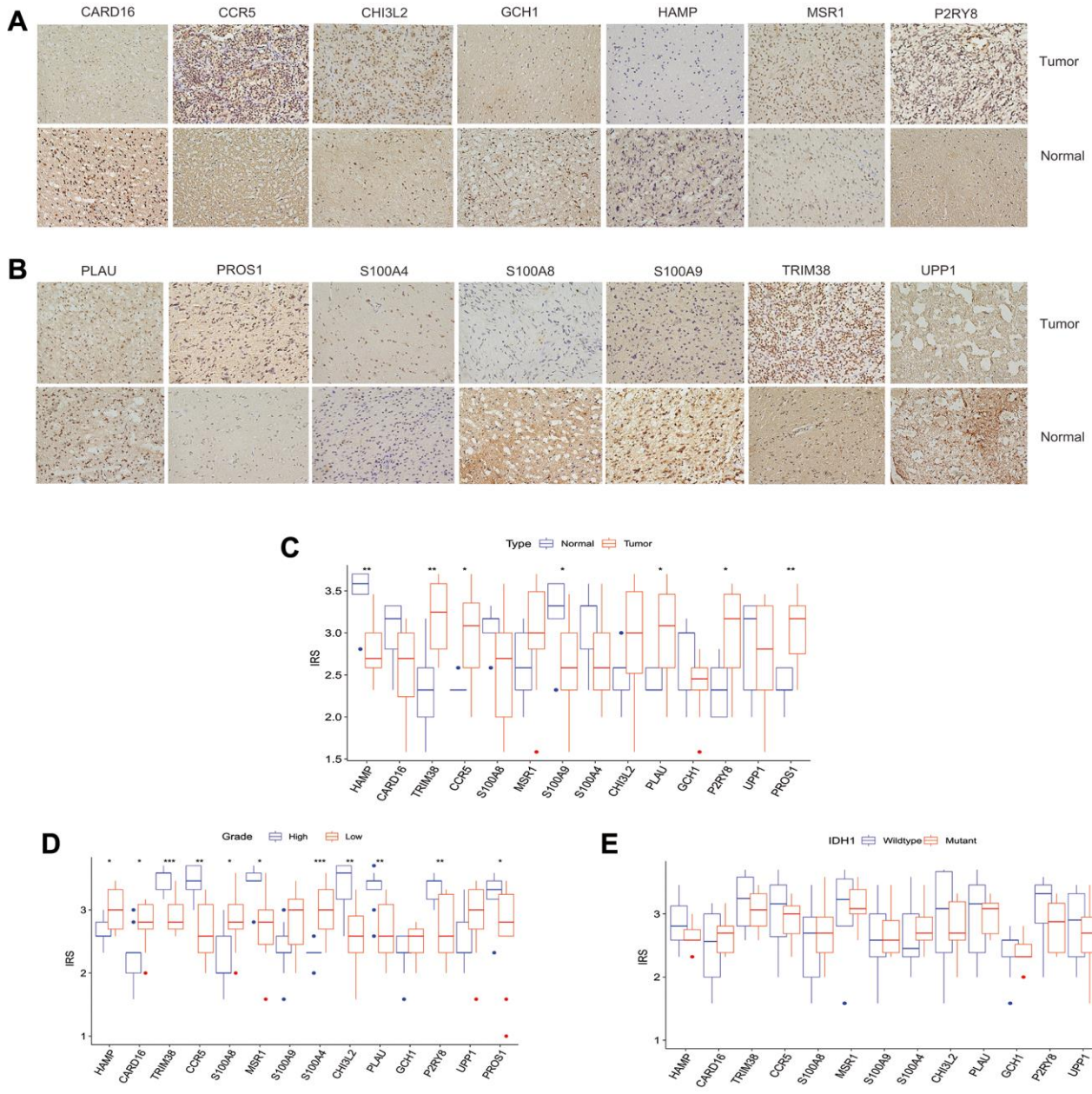

Figure 9. The clinical significance of intersection proteins between TLS subtypes in glioma confirmed by immunohistochemistry. (**A** and **B**) The typical image showed the expression status of the 14 intersection proteins in glioma and normal tissues. (**C**) The expression status of the 14 intersection proteins between glioma and normal tissues. (**D**) The expression of the 14 proteins associated with tumor grade. (**E**) the expression of the 14 proteins associated with IDH1 mutation status.

Furthermore, TLSs have been reported to be associated with increased T cell infiltration [11]. As a result, we evaluated the relationship between distinct TLS subtypes and drug sensitivity to understand the effect of the TLS subtype on the drug response. We screened a variety of sensitive drugs for each TLS subtype. However, whether these drugs play an important role in the treatment of glioma based on the TLS subtype needs to be verified by further studies. Regulating the formation of TLS to promote the immunotherapy effect has become one of the priorities of tumor immunotherapy [28], which suggested that TLS could be exploited therapeutically, in particular for nonresponsive, immune "cold" cancers. However, TLS formation induced by immunostimulatory agonistic CD40 antibodies was observed to impair the efficacy of anti-PD-1 antibodies (αPD-1) in murine gliomas through the accumulation of CD11b-expressing B cells, which may inhibit CD8+ T cell responses [11]. Thus, it is important to identify the potential reagents to improve the TLS formation with increasing anti-tumorigenic immune cells but not pro-tumorigenic immune cells including M2 polarized macrophages, T-helper 2 cells, myeloid-derived suppressor cells, and regulatory T cells.

Last, the calculated riskscore based on the intersection gene among TLS subtype suggested that patients with high riskscores had shorter overall survival compared with that of patients with low riskscore, which further demonstrated the prognostic relevance of TLS signature. The 14 proteins found significantly differentially expressed between TLS clusters. TRIM38, CCR5, PLAU, P2RY8, and PROS1 were upregulated in glioma tissues, while HAMP and S100A9 were downregulated. We observed that PROS1, P2RY8, PLAU, CHI3L2, MSR1, CCR5, TRIM38, HAMP, CARD16, and S100A8 were associated with tumor grade. Further studies with a large sample size should be performed to confirm our results or unearth the corresponding cellular mechanism. The results and conclusions of the present study were primarily obtained via bioinformatics analysis based on TCGA, CGGA, and GSE16011 cohorts. The distribution of TLS and modulation of TLS formation in glioma tissues should be explored in future studies.

In summary, we stratified gliomas into three subtypes according to the unsupervised clustering of TLS signature expression profiles. The relevance of clinical characteristics, immune infiltration, tumor microenvironment, potential biological functions, and drug sensitivity were investigated. The findings may shed light on the molecular subtypes of gliomas and deepen our understanding of TLS heterogeneity in gliomas. The study presents a method of stratification for the therapeutic induction of specific TLSs to enhance anti-cancer immunotherapy.

METHODS

Patients and datasets

A total of 2090 glioma patients from public datasets including The Cancer Genome Atlas (TCGA), Chinese Glioma Genome Atlas (CGGA), and GSE16011 were enrolled in this study. For the TCGA dataset (http://cancergenome.nih.gov/), we downloaded the RNA-seq data, copy number alterations (CNAs), somatic mutations, and the corresponding clinical information [29]. The CGGA database included two RNA-seq datasets and one microarray dataset with the corresponding clinical information (http://www.cgga.org.cn). The RNA-seq, microarray datasets, and the corresponding clinical information were extracted [29]. We combined the two RNA-seq datasets and named it CGGA_cohort1, and the microarray dataset was named CGGA_cohort2. For the GSE16011 cohort, we extracted microarray data accompanied with clinical information from the GEO database (https://www.ncbi.nlm.nih.gov/geo/) [29]. The gene expression data of normal brain tissues were extracted from Genotype-Tissue Expression (GTEx, https://gtexportal.org/) [30].

Construction and validation of TLS subtypes

Recently, Catherine et al. summarized the gene signatures required for TLS analysis identified from the transcriptomic analyses of human cancers, which include 12 chemokine signatures (CCL2, CCL3, CCL4, CCL5, CCL8, CCL18, CCL19, CCL21, CXCL9, CXCL8, CXCL11, CXCL13), T_{FH} cell signatures (CXCL13, CD200, FBLN7, ICOS, SGPP2, SH2D1A, TIGIT, PDCD1), T_H1 cell and B cell signatures (CD4, CCR5, CXCR3, CSF2, IGSF6, IL2RA, CD38, CD40, CD5, MS4A1, SDC1, GFI1, IL1R1, IL1R2, IL10, CCL20, IRF4, TRAF6, STAT5A), a plasma cell signature (TNFRSF17), and a CXCL13 signature (CXCL13) [6]. To ensure that all TLS signatures can be detected, consensus clustering was performed based on the 12 chemokine signatures, T_{FH} cell signatures, T_H1 cell and B cell signatures, plasma cell signature, and CXCL13 signature to identify robust clusters of glioma. The optimal k was assessed using a consensus heatmap and the cumulative distribution function. We used the TCGA database as the training cohort to train a partition around medoids (PAM) classifier and validate the TLS subtypes in CGGA_cohort1, CGGA_cohort2, and GSE16011. The reproducibility and similarity of the TLS subtypes among the training and validation cohorts were assessed by the R package "clusterRepro".

Gene set variation analysis (GSVA) and functional annotation

The potential biological functions related to TLS subtypes were enriched by gene set variation analysis (GSVA) using the R package "GSVA" [31]. We downloaded the gene set "h.all.v7.2" and "c2.cp.kegg.v7.1" from MsigDB database to perform GSVA analysis. The functional annotation of the TLS related genes was conducted by clusterProfiler R Package [32].

Calculation of immune cell infiltration for different TLS subtypes

We used ESTIMATE to calculate the stromal score (stromal content), tumor purity, and immune score (immune cell infiltration) for each glioma sample [33]. Single-sample GSEA (ssGSEA) was performed to estimate the infiltration levels of 23 immune signatures by using the R package "GSVA" [31, 34]. The genes were used to define the immune cell were summarized in Supplementary Table 7.

Association analysis of TLS subtype and drug sensitivity

The R package "pRRophetic" was employed to assess the sensitivity of these three distinct glioma subtypes [35]. The maximum inhibitory concentration (IC50) and prediction accuracy were evaluated by algorithm through 10-fold crossvalidation and ridge regression of the Dependent Cancer Drug Sensitivity Genomics (GDSC) database (https://www.cancerrxgene.org/).

Calculation of riskscore based on intersection genes among TLS subtypes

Differentially expressed genes (DEGs) were identified by comparing three TLS subtypes, and intersection genes were identified using the R package "Venn". The intersection genes from TCGA, CGGA_cohort1, CGGA_cohort2, and GSE16011 were then analyzed again using the R package "Venn". The TCGA database and GTEx were used to evaluate the expression of the intersection genes in tumor and normal tissues. Genes with a false discovery rate (FDR) <0.05 and a log2 fold change (FC) >1 were defined as genes with differential expression [32]. The TCGA database was used to select genes related to prognosis. Prognosis-related genes with differential expression were used to calculate riskscores via LASSO regression in the training cohort of TCGA. Riskscore were then calculated in the testing cohorts including CGGA_cohort1, CGGA_cohort2, and GSE16011 [36]. The prognostic role of the riskscore of glioma patients was assessed in the training and testing cohorts by univariate and multivariate Cox proportional hazards regression analyses.

Immunohistochemistry

A total of 20 cases of glioma and 5 normal tissues were collected to validate the expression of key proteins found significantly differentially expressed between TLS clusters from our hospital. The clinical information includes gender, age, tumor location, histology, and the common molecule change such as isocitrate dehydrogenase (IDH). The ethical committee of the affiliated hospital of Guizhou medical university approved this study protocol, and informed consent was obtained from patients. The 14 proteins expressed between TLS clusters were assessed by immunohistochemistry staining based on the protocol instruction [37]. Put simply, the thickness of the tissue section is 8 μm. Dewaxing with xylene and rehydration was used to reduce ethanol concentration. Antigen recovery was obtained by boiling slices on 10 mm citrate buffer for 20 minutes. The slices were incubated with background Sniper (Biocare Medical) for 30 minutes at room temperature after the endogenous peroxidase with 3% catalase was blocked in methanol. The sections were then incubated with primary antibodies of the HAMP(1:200, Abcam, #ab31875), CARD16 (1:200, Abcam,#aa1-100), TRIM38 (1:100, Proteintech, #O00635), CCR5(1:200, R&D Systems, #P51681), S100A8(1:250, Abcam,#D3DV36), MSR1 (1:200, Bio-Rad, #E9QNQ5), S100A9 (1:200, Bio-Rad, #D3DV36), S100A4(1:400, Dako, #P20066), CHI3L2 (1:300, GeneTex, #A6NNY3), PLAU(1:100, Proteintech,#P00749), GCH1 (1:200, Abnova, #P30793), P2RY8 (1:500, R&D Systems, #BAA92159), UPP1 (1:300, MilliporeSigma, #Q15362), PROS1 (1:300, Developmental Studies Hybridoma Bank, #P29617) at 4°C overnight with a working concentration of 1:100, respectively. The immunoreaction score (IRS) was used to assess the immunohistochemical staining results. The IRS was defined as the percentage of positive cells X staining intensity, which was ranged from 0–12 [38]. The clinical association of IRS for these 14 proteins were evaluated.

Data analysis

R software (version 4.0.4) was used to perform all analyses. Differences in clinical and molecular features between subtypes were compared by the Chi-square test. One-way ANOVA was carried out for the comparison of three groups. A p-value < or = 0.05 was defined as statistically significant.

Ethics approval and informed consent

The experimental verification of this study was approved by the ethics committee of the affiliated hospital of Guizhou medical university.

Abbreviations

TLS: Tertiary lymphoid structure; TCGA: The Cancer Genome Atlas; CNGA: Chinese Glioma Genome Atlas; Genotype-Tissue Expression; CNAs: copy number alterations; DEGs: Differentially expressed genes; FDR: false discovery rate; FDCs: Follicular dendritic cells; GCs: germinal centers; HEVs: endothelial venules; IRS: immunoreaction score.

AUTHOR CONTRIBUTIONS

Xingwang Zhou and Liangzhao Chu conceived and designed the project; Xingwang Zhou, Wenyan Li, and Hua Yang collected the data; Xingwang Zhou, Hua Yang, Liangzhao Chu, Jie Yang, Yimin Chen, Xiaolan Qi performed the interpretation of data and statistical analysis; Xingwang Zhou carried out the immunohistochemistry, Xingwang Zhou wrote the manuscript; Liangzhao Chu and Hua Yang revised the paper. All authors read and approved the final manuscript.

ACKNOWLEDGMENTS

We would like to acknowledge the researchers' contribution to the TCGA, CGGA, GEO databases.

CONFLICTS OF INTEREST

The authors declare no conflicts of interest related to this study.

REFERENCES

1. Colman H. Adult Gliomas. Continuum (Minneap Minn). 2020; 26:1452–75. https://doi.org/10.1212/CON.0000000000000935 PMID:33273168

2. Adamson C, Kanu OO, Mehta AI, Di C, Lin N, Mattox AK, Bigner DD. Glioblastoma multiforme: a review of where we have been and where we are going. Expert Opin Investig Drugs. 2009; 18:1061–83. https://doi.org/10.1517/13543780903052764 PMID:19555299

3. McClelland S 3rd, Sosanya O, Mitin T, Degnin C, Chen Y, Attia A, Suh JH, Jaboin JJ. Application of tumor treating fields for newly diagnosed glioblastoma: understanding of nationwide practice patterns. J Neurooncol. 2018; 140:155–8. https://doi.org/10.1007/s11060-018-2945-y PMID:29987746

4. Sanmamed MF, Chen L. A Paradigm Shift in Cancer Immunotherapy: From Enhancement to Normalization. Cell. 2019; 176:677. https://doi.org/10.1016/j.cell.2019.01.008 PMID:30682374

5. Yang T, Kong Z, Ma W. PD-1/PD-L1 immune checkpoint inhibitors in glioblastoma: clinical studies, challenges and potential. Hum Vaccin Immunother. 2021; 17:546–53. https://doi.org/10.1080/21645515.2020.1782692 PMID:32643507

6. Sautès-Fridman C, Petitprez F, Calderaro J, Fridman WH. Tertiary lymphoid structures in the era of cancer immunotherapy. Nat Rev Cancer. 2019; 19:307–25. https://doi.org/10.1038/s41568-019-0144-6 PMID:31092904

7. Martinet L, Garrido I, Filleron T, Le Guellec S, Bellard E, Fournie JJ, Rochaix P, Girard JP. Human solid tumors contain high endothelial venules: association with T- and B-lymphocyte infiltration and favorable prognosis in breast cancer. Cancer Res. 2011; 71:5678–87. https://doi.org/10.1158/0008-5472.CAN-11-0431 PMID:21846823

8. Ruffin AT, Cillo AR, Tabib T, Liu A, Onkar S, Kunning SR, Lampenfeld C, Atiya HI, Abecassis I, Kürten CHL, Qi Z, Soose R, Duvvuri U, et al. B cell signatures and tertiary lymphoid structures contribute to outcome in head and neck squamous cell carcinoma. Nat Commun. 2021; 12:3349. https://doi.org/10.1038/s41467-021-23355-x PMID:34099645

9. Tang J, Ramis-Cabrer D, Curull V, Wang X, Mateu-Jiménez M, Pijuan L, Duran X, Qin L, Rodríguez-Fuster A, Aguiló R, Barreiro E. B Cells and Tertiary Lymphoid Structures Influence Survival in Lung Cancer Patients with Resectable Tumors. Cancers (Basel). 2020; 12:2644. https://doi.org/10.3390/cancers12092644 PMID:32947928

10. Petitprez F, de Reyniès A, Keung EZ, Chen TW, Sun CM, Calderaro J, Jeng YM, Hsiao LP, Lacroix L, Bougoüin A, Moreira M, Lacroix G, Natario I, et al. B cells are associated with survival and immunotherapy response in sarcoma. Nature. 2020; 577:556–60. https://doi.org/10.1038/s41586-019-1906-8 PMID:31942077

11. van Hooren L, Vaccaro A, Ramachandran M, Vazaios K, Libard S, van de Walle T, Georganaki M, Huang H, Pietilä I, Lau J, Ulvmar MH, Karlsson MCI, Zetterling M, et al. Agonistic CD40 therapy induces tertiary

lymphoid structures but impairs responses to checkpoint blockade in glioma. Nat Commun. 2021; 12:4127.
https://doi.org/10.1038/s41467-021-24347-7
PMID:34226552

12. Lynch KT, Young SJ, Meneveau MO, Wages NA, Engelhard VH, Slingluff CL Jr, Mauldin IS. Heterogeneity in tertiary lymphoid structure B-cells correlates with patient survival in metastatic melanoma. J Immunother Cancer. 2021; 9:e002273.
https://doi.org/10.1136/jitc-2020-002273
PMID:34103353

13. Zhou L, Xu B, Liu Y, Wang Z. Tertiary lymphoid structure signatures are associated with survival and immunotherapy response in muscle-invasive bladder cancer. Oncoimmunology. 2021; 10:1915574.
https://doi.org/10.1080/2162402X.2021.1915574
PMID:34104539

14. Trüb M, Zippelius A. Tertiary Lymphoid Structures as a Predictive Biomarker of Response to Cancer Immunotherapies. Front Immunol. 2021; 12:674565.
https://doi.org/10.3389/fimmu.2021.674565
PMID:34054861

15. Siliņa K, Soltermann A, Attar FM, Casanova R, Uckeley ZM, Thut H, Wandres M, Isajevs S, Cheng P, Curioni-Fontecedro A, Foukas P, Levesque MP, Moch H, et al. Germinal Centers Determine the Prognostic Relevance of Tertiary Lymphoid Structures and Are Impaired by Corticosteroids in Lung Squamous Cell Carcinoma. Cancer Res. 2018; 78:1308–20.
https://doi.org/10.1158/0008-5472.CAN-17-1987
PMID:29279354

16. Germain C, Gnjatic S, Dieu-Nosjean MC. Tertiary Lymphoid Structure-Associated B Cells are Key Players in Anti-Tumor Immunity. Front Immunol. 2015; 6:67.
https://doi.org/10.3389/fimmu.2015.00067
PMID:25755654

17. Hiraoka N, Ino Y, Yamazaki-Itoh R, Kanai Y, Kosuge T, Shimada K. Intratumoral tertiary lymphoid organ is a favourable prognosticator in patients with pancreatic cancer. Br J Cancer. 2015; 112:1782–90.
https://doi.org/10.1038/bjc.2015.145
PMID:25942397

18. Calderaro J, Petitprez F, Becht E, Laurent A, Hirsch TZ, Rousseau B, Luciani A, Amaddeo G, Derman J, Charpy C, Zucman-Rossi J, Fridman WH, Sautès-Fridman C. Intra-tumoral tertiary lymphoid structures are associated with a low risk of early recurrence of hepatocellular carcinoma. J Hepatol. 2019; 70:58–65.
https://doi.org/10.1016/j.jhep.2018.09.003
PMID:30213589

19. Messina JL, Fenstermacher DA, Eschrich S, Qu X, Berglund AE, Lloyd MC, Schell MJ, Sondak VK, Weber JS, Mulé JJ. 12-Chemokine gene signature identifies lymph node-like structures in melanoma: potential for patient selection for immunotherapy? Sci Rep. 2012; 2:765.
https://doi.org/10.1038/srep00765
PMID:23097687

20. Lucchesi D, Bombardieri M. The role of viruses in autoreactive B cell activation within tertiary lymphoid structures in autoimmune diseases. J Leukoc Biol. 2013; 94:1191–9.
https://doi.org/10.1189/jlb.0413240
PMID:23812327

21. Sautès-Fridman C, Lawand M, Giraldo NA, Kaplon H, Germain C, Fridman WH, Dieu-Nosjean MC. Tertiary Lymphoid Structures in Cancers: Prognostic Value, Regulation, and Manipulation for Therapeutic Intervention. Front Immunol. 2016; 7:407.
https://doi.org/10.3389/fimmu.2016.00407
PMID:27752258

22. Selitsky SR, Mose LE, Smith CC, Chai S, Hoadley KA, Dittmer DP, Moschos SJ, Parker JS, Vincent BG. Prognostic value of B cells in cutaneous melanoma. Genome Med. 2019; 11:36.
https://doi.org/10.1186/s13073-019-0647-5
PMID:31138334

23. Cipponi A, Mercier M, Seremet T, Baurain JF, Théate I, van den Oord J, Stas M, Boon T, Coulie PG, van Baren N. Neogenesis of lymphoid structures and antibody responses occur in human melanoma metastases. Cancer Res. 2012; 72:3997–4007.
https://doi.org/10.1158/0008-5472.CAN-12-1377
PMID:22850419

24. Goc J, Germain C, Vo-Bourgais TK, Lupo A, Klein C, Knockaert S, de Chaisemartin L, Ouakrim H, Becht E, Alifano M, Validire P, Remark R, Hammond SA, et al. Dendritic cells in tumor-associated tertiary lymphoid structures signal a Th1 cytotoxic immune contexture and license the positive prognostic value of infiltrating CD8+ T cells. Cancer Res. 2014; 74:705–15.
https://doi.org/10.1158/0008-5472.CAN-13-1342
PMID:24366885

25. Hennequin A, Derangère V, Boidot R, Apetoh L, Vincent J, Orry D, Fraisse J, Causeret S, Martin F, Arnould L, Beltjens F, Ghiringhelli F, Ladoire S. Tumor infiltration by Tbet+ effector T cells and CD20+ B cells is associated with survival in gastric cancer patients. Oncoimmunology. 2015; 5:e1054598.
https://doi.org/10.1080/2162402X.2015.1054598
PMID:27057426

26. Gu-Trantien C, Loi S, Garaud S, Equeter C, Libin M, de Wind A, Ravoet M, Le Buanec H, Sibille C, Manfouo-

Foutsop G, Veys I, Haibe-Kains B, Singhal SK, et al. CD4+ follicular helper T cell infiltration predicts breast cancer survival. J Clin Invest. 2013; 123:2873–92. https://doi.org/10.1172/JCI67428 PMID:23778140

27. Truxova I, Kasikova L, Hensler M, Skapa P, Laco J, Pecen L, Belicova L, Praznovec I, Halaska MJ, Brtnicky T, Salkova E, Rob L, Kodet R, et al. Mature dendritic cells correlate with favorable immune infiltrate and improved prognosis in ovarian carcinoma patients. J Immunother Cancer. 2018; 6:139. https://doi.org/10.1186/s40425-018-0446-3 PMID:30526667

28. Johansson-Percival A, Ganss R. Therapeutic Induction of Tertiary Lymphoid Structures in Cancer Through Stromal Remodeling. Front Immunol. 2021; 12:674375. https://doi.org/10.3389/fimmu.2021.674375 PMID:34122434

29. Ceccarelli M, Barthel FP, Malta TM, Sabedot TS, Salama SR, Murray BA, Morozova O, Newton Y, Radenbaugh A, Pagnotta SM, Anjum S, Wang J, Manyam G, et al, and TCGA Research Network. Molecular Profiling Reveals Biologically Discrete Subsets and Pathways of Progression in Diffuse Glioma. Cell. 2016; 164:550–63. https://doi.org/10.1016/j.cell.2015.12.028 PMID:26824661

30. Lonsdale J, Thomas J, Salvatore M, Phillips R, Lo E, Shad S, Hasz R, Walters G, Garcia F, Young N, Foster B, Moser M, Karasik E, et al, and GTEx Consortium. The Genotype-Tissue Expression (GTEx) project. Nat Genet. 2013; 45:580–5. https://doi.org/10.1038/ng.2653 PMID:23715323

31. Hänzelmann S, Castelo R, Guinney J. GSVA: gene set variation analysis for microarray and RNA-seq data. BMC Bioinformatics. 2013; 14:7. https://doi.org/10.1186/1471-2105-14-7 PMID:23323831

32. Yu G, Wang LG, Han Y, He QY. clusterProfiler: an R package for comparing biological themes among gene clusters. OMICS. 2012; 16:284–7. https://doi.org/10.1089/omi.2011.0118 PMID:22455463

33. Yoshihara K, Shahmoradgoli M, Martínez E, Vegesna R, Kim H, Torres-Garcia W, Treviño V, Shen H, Laird PW, Levine DA, Carter SL, Getz G, Stemke-Hale K, et al. Inferring tumour purity and stromal and immune cell admixture from expression data. Nat Commun. 2013; 4:2612. https://doi.org/10.1038/ncomms3612 PMID:24113773

34. He Y, Jiang Z, Chen C, Wang X. Classification of triple-negative breast cancers based on Immunogenomic profiling. J Exp Clin Cancer Res. 2018; 37:327. https://doi.org/10.1186/s13046-018-1002-1 PMID:30594216

35. Geeleher P, Cox N, Huang RS. pRRophetic: an R package for prediction of clinical chemotherapeutic response from tumor gene expression levels. PLoS One. 2014; 9:e107468. https://doi.org/10.1371/journal.pone.0107468 PMID:25229481

36. Chen H, Yao J, Bao R, Dong Y, Zhang T, Du Y, Wang G, Ni D, Xun Z, Niu X, Ye Y, Li HB. Cross-talk of four types of RNA modification writers defines tumor microenvironment and pharmacogenomic landscape in colorectal cancer. Mol Cancer. 2021; 20:29. https://doi.org/10.1186/s12943-021-01322-w PMID:33557837

37. Dadhania V, Zhang M, Zhang L, Bondaruk J, Majewski T, Siefker-Radtke A, Guo CC, Dinney C, Cogdell DE, Zhang S, Lee S, Lee JG, Weinstein JN, et al. Meta-Analysis of the Luminal and Basal Subtypes of Bladder Cancer and the Identification of Signature Immunohistochemical Markers for Clinical Use. EBioMedicine. 2016; 12:105–17. https://doi.org/10.1016/j.ebiom.2016.08.036 PMID:27612592

38. Yu L, Xiao Z, Tu H, Tong B, Chen S. The expression and prognostic significance of Drp1 in lung cancer: A bioinformatics analysis and immunohistochemistry. Medicine (Baltimore). 2019; 98:e18228. https://doi.org/10.1097/MD.0000000000018228 PMID:31770286

SUPPLEMENTARY MATERIALS

Supplementary Figures

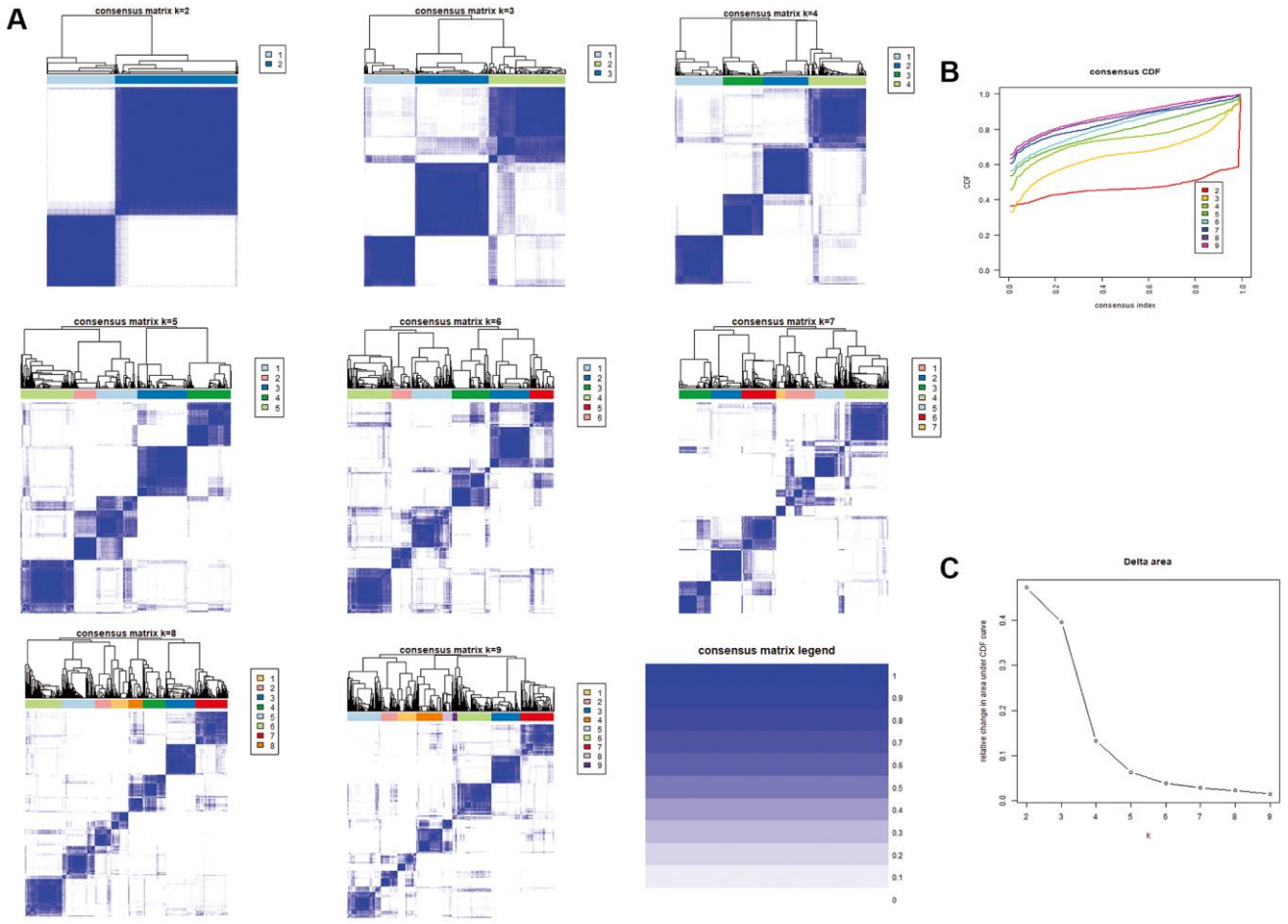

Supplementary Figure 1. Consensus clustering based in TLS gene expression of TCGA glioma. (**A**) Clustering matrix for k = 2 to k = 9. (**B**) CDF (cumulative distribution function) curve for k = 2 to k = 10. (**C**) Relative change in area under CDF curve for k = 2 to k = 10.

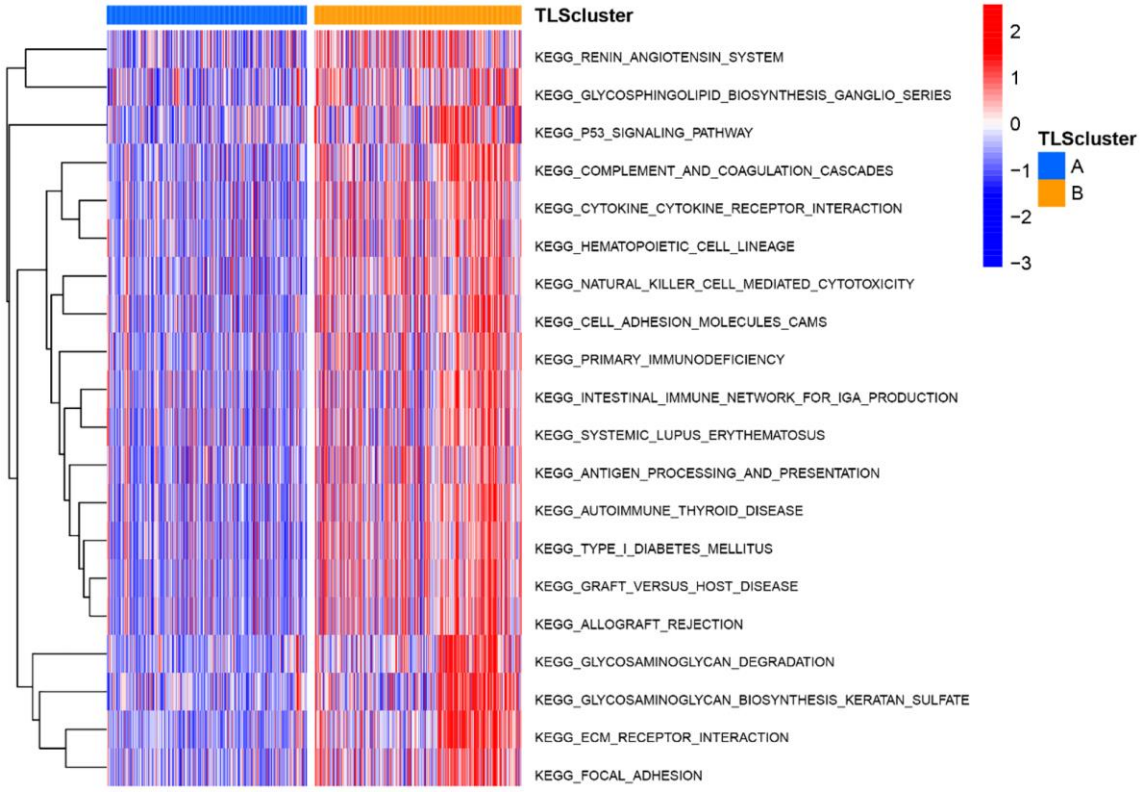

Supplementary Figure 2. The top 20 potential biological functions between subtype A and B in TCGA.

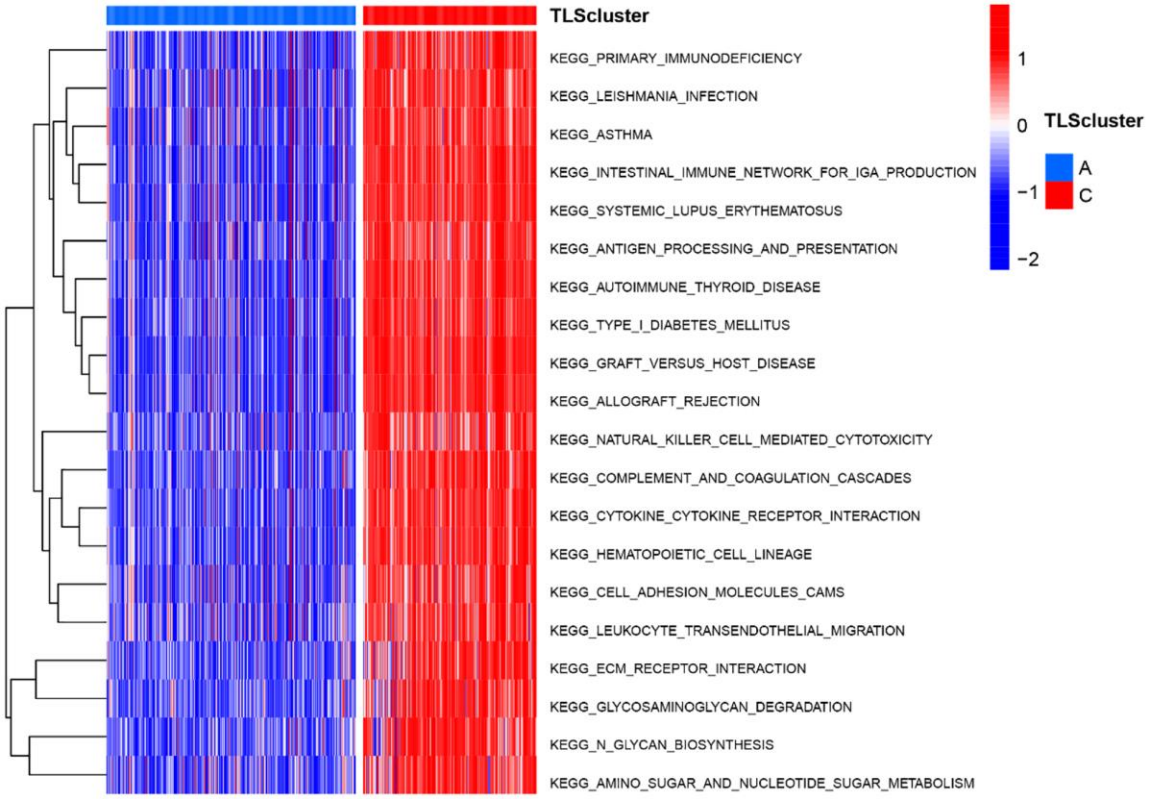

Supplementary Figure 3. The top 20 potential biological functions between subtype A and C in TCGA.

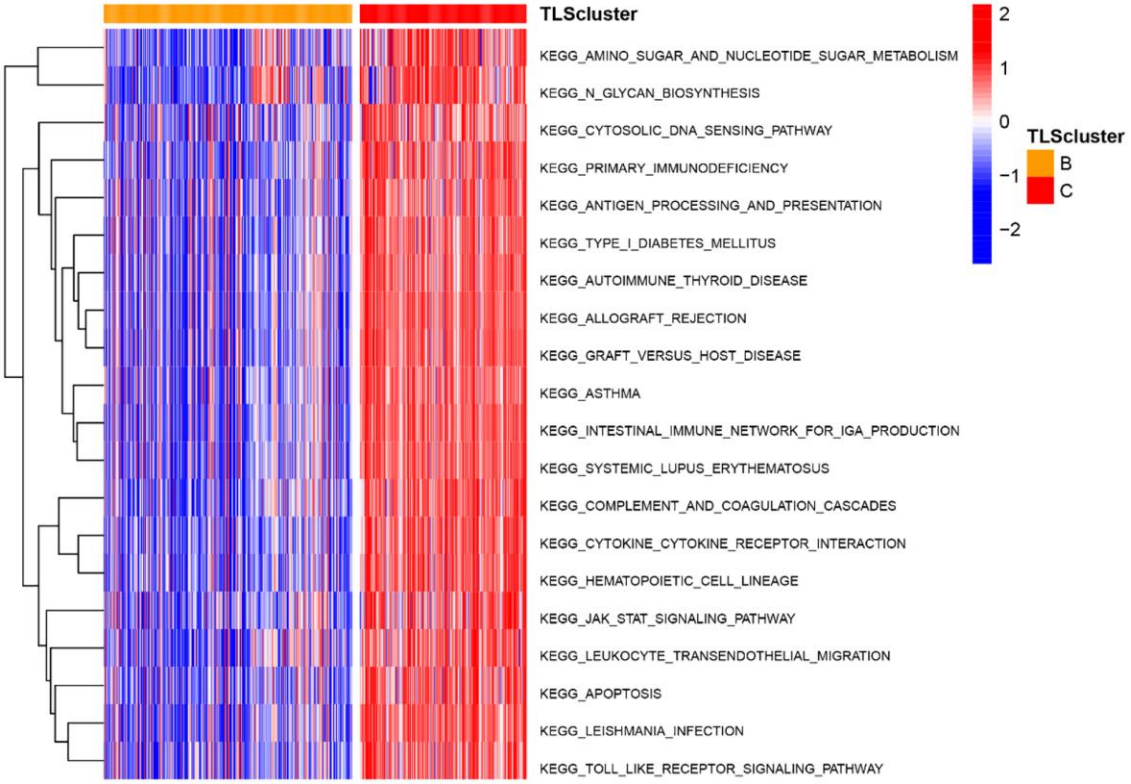

Supplementary Figure 4. The top 20 potential biological functions between subtype B and C in TCGA.

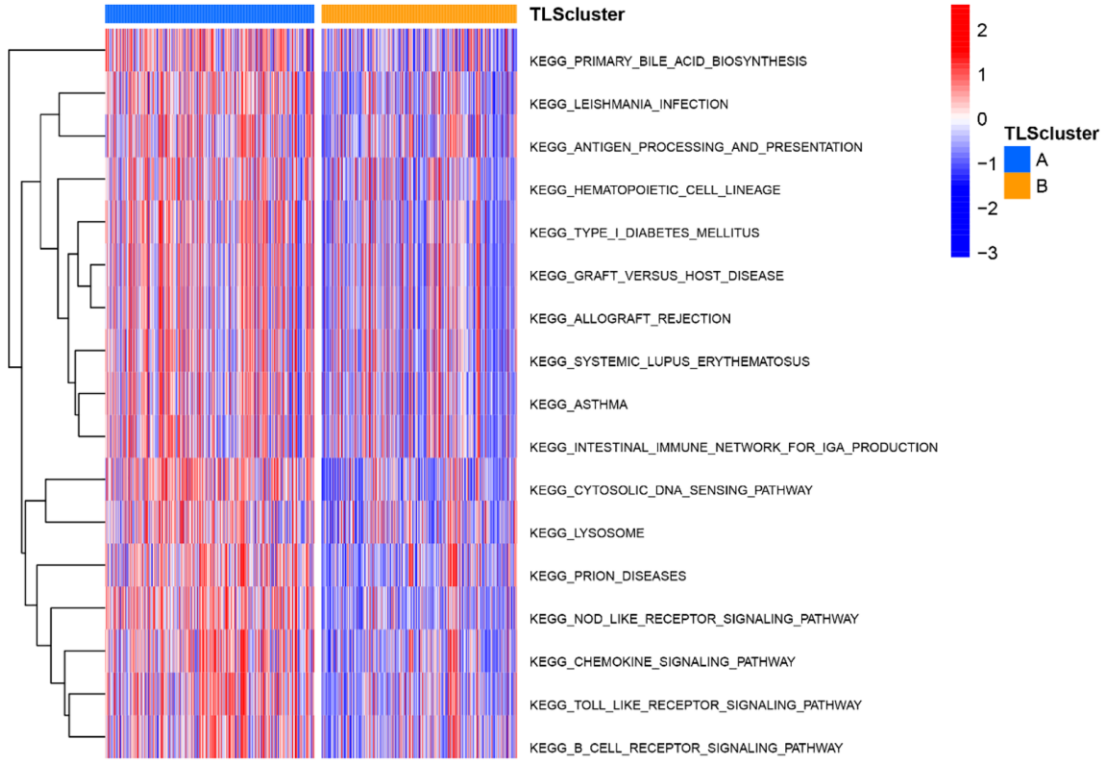

Supplementary Figure 5. The top 20 potential biological functions between subtype A and B in CGGA_cohort1.

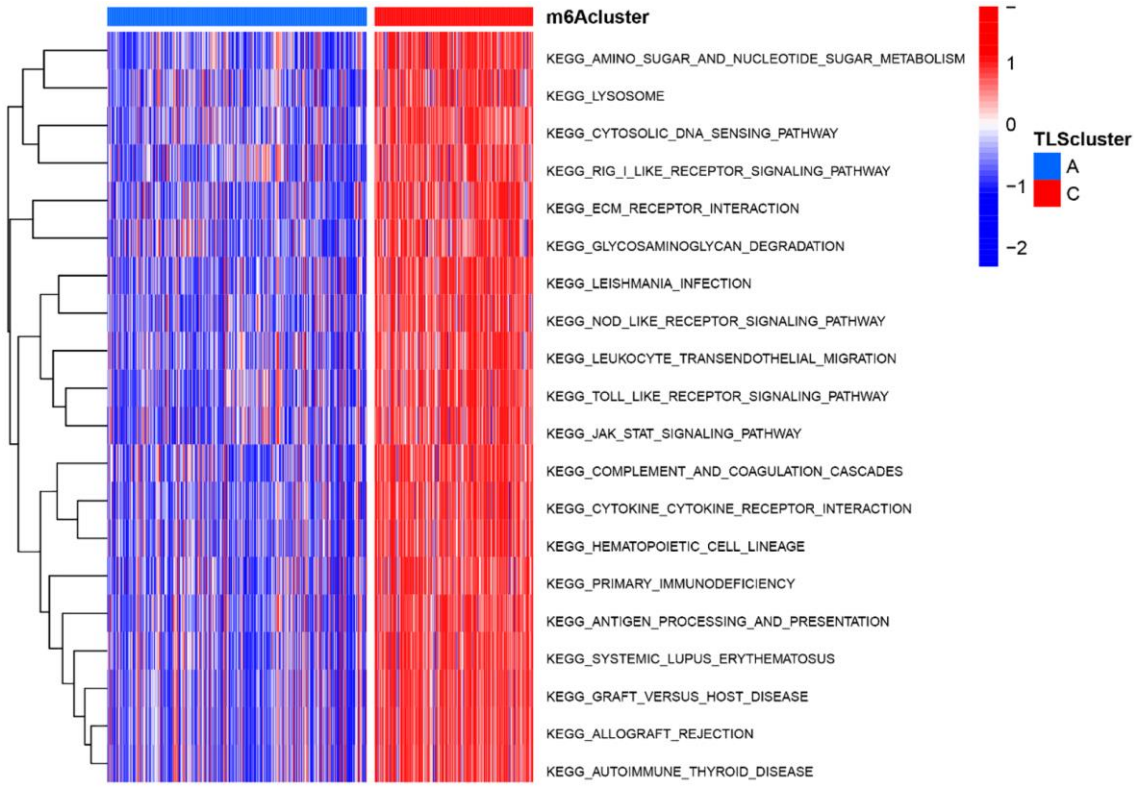

Supplementary Figure 6. The top 20 potential biological functions between subtype A and C in CGGA_cohort1.

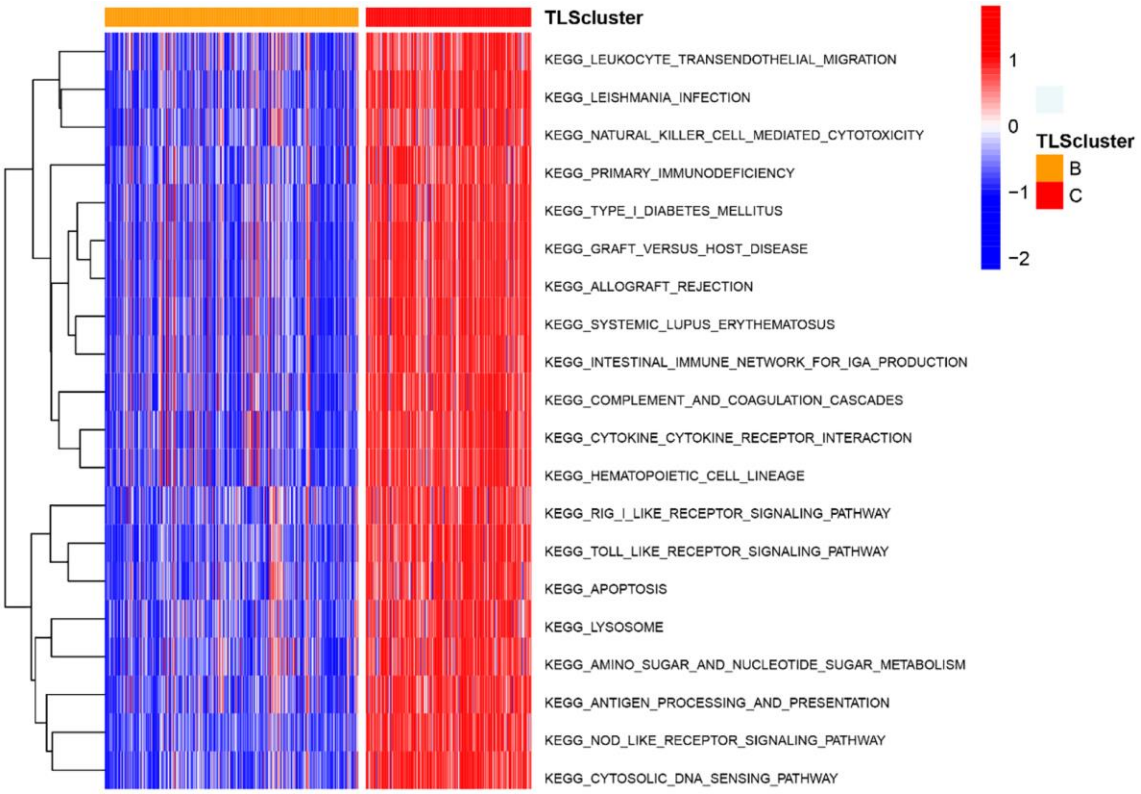

Supplementary Figure 7. The top 20 potential biological functions between subtype B and C in CGGA_cohort1.

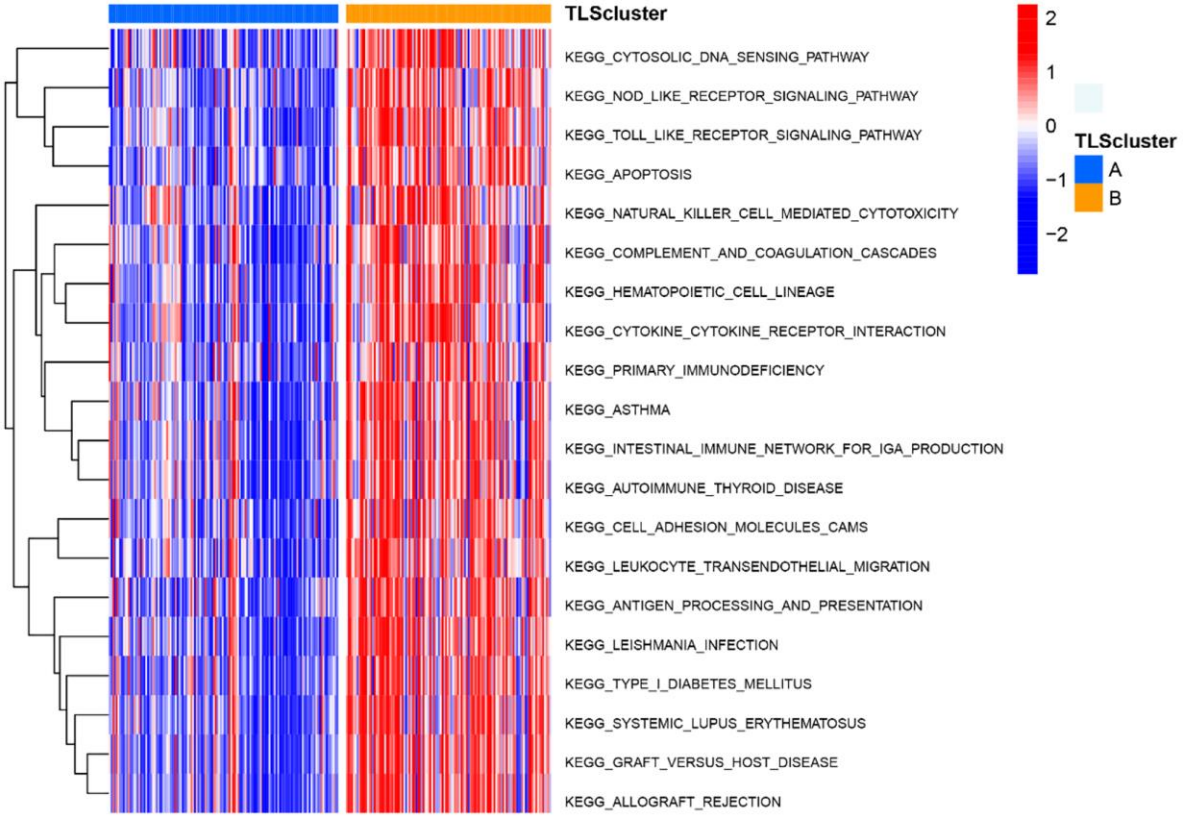

Supplementary Figure 8. The top 20 potential biological functions between subtype A and B in CGGA_cohort2.

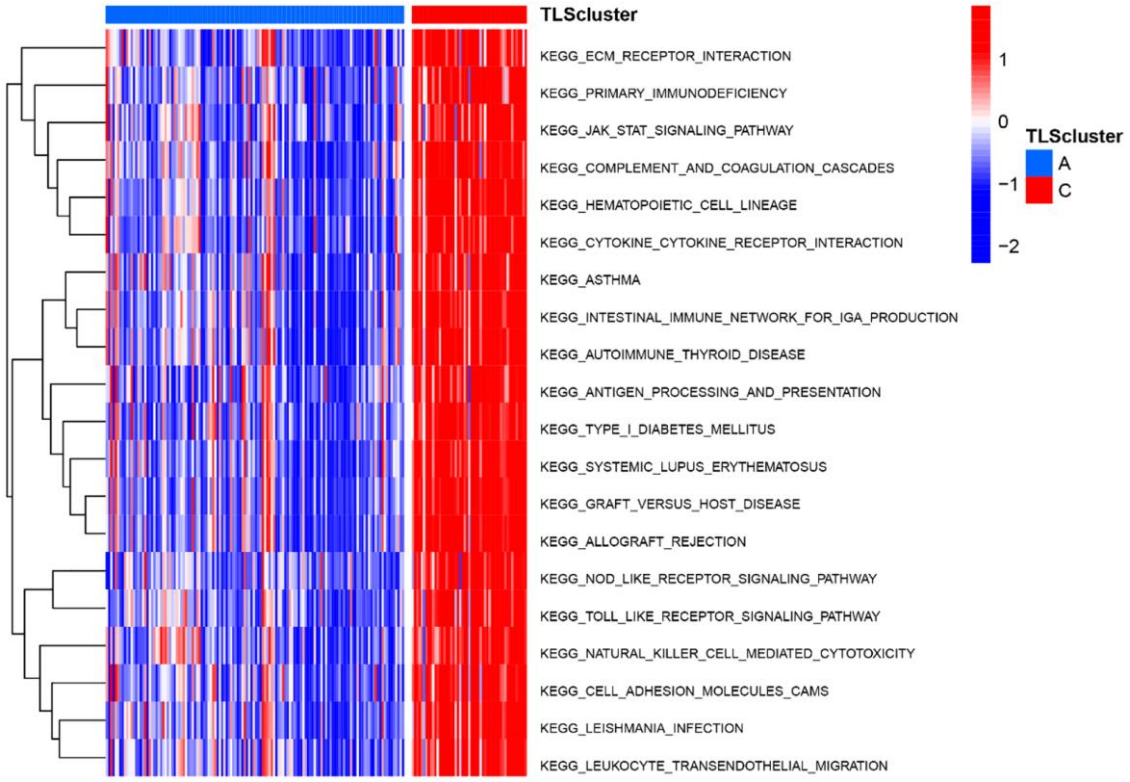

Supplementary Figure 9. The top 20 potential biological functions between subtype A and C in CGGA_cohort2.

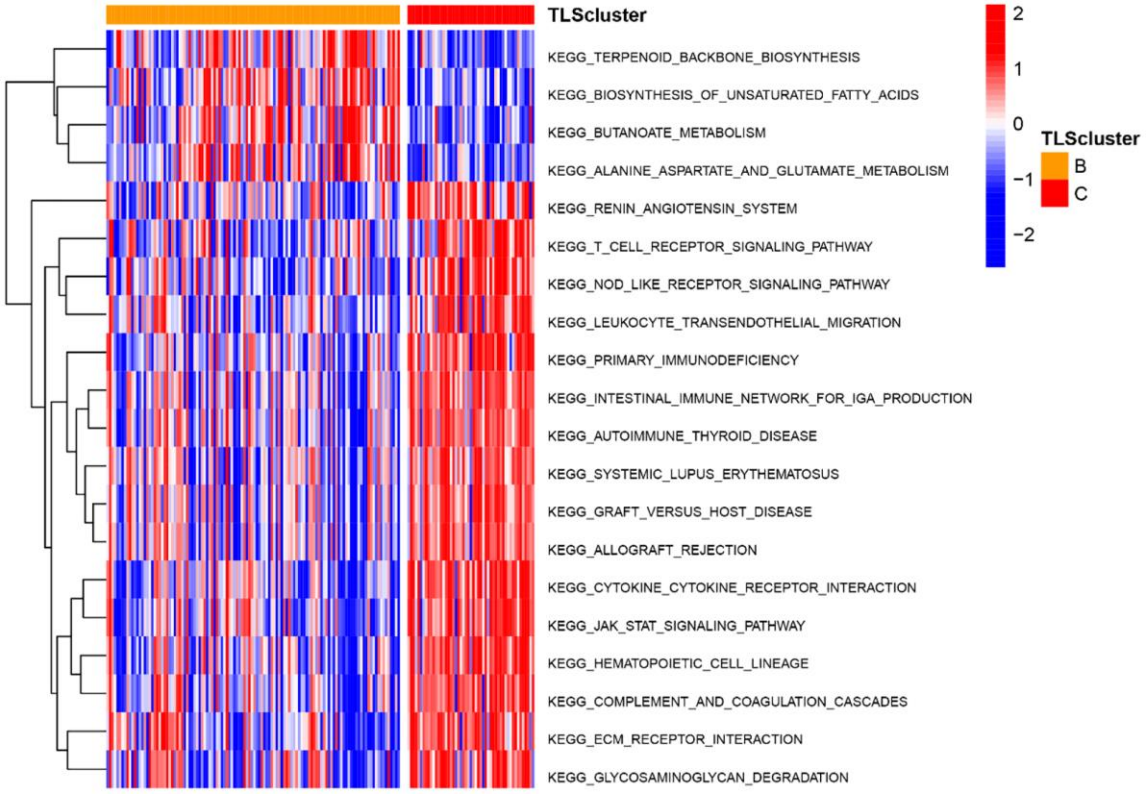

Supplementary Figure 10. The top 20 potential biological functions between subtype B and C in CGGA_cohort2.

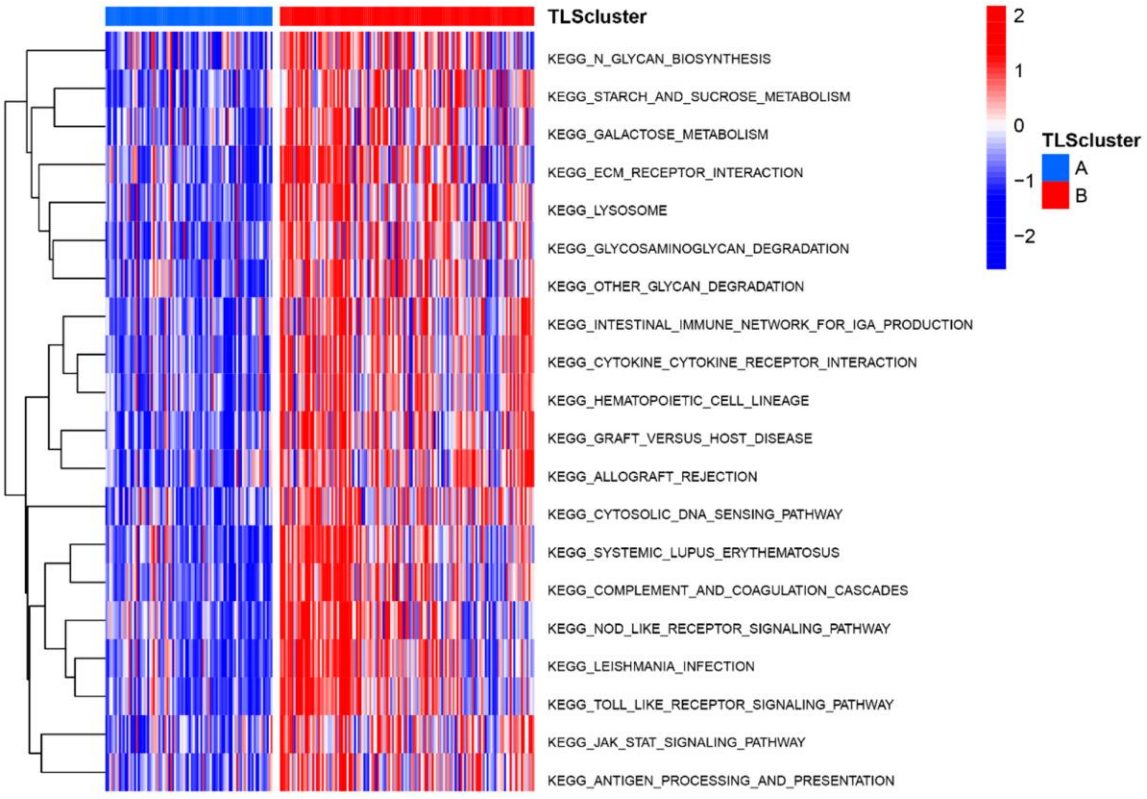

Supplementary Figure 11. The top 20 potential biological functions between subtype A and B in GSE16011.

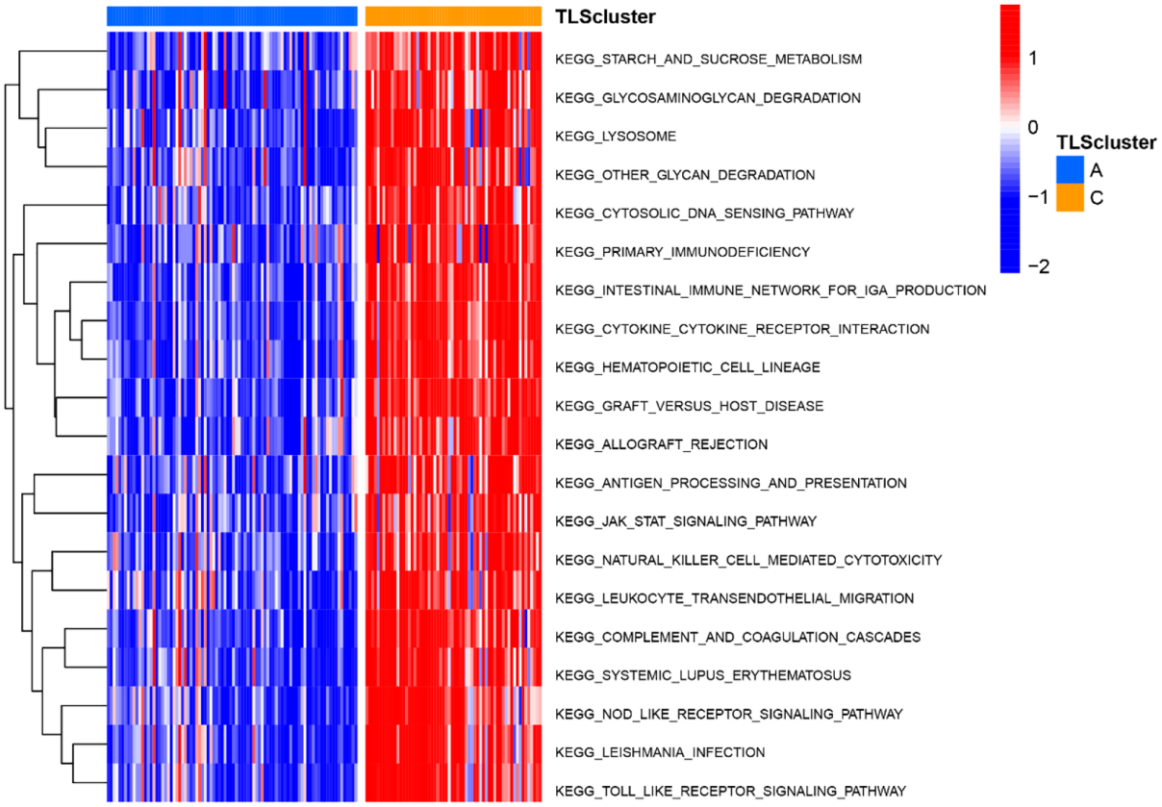

Supplementary Figure 12. The top 20 potential biological functions between subtype A and C in GSE16011.

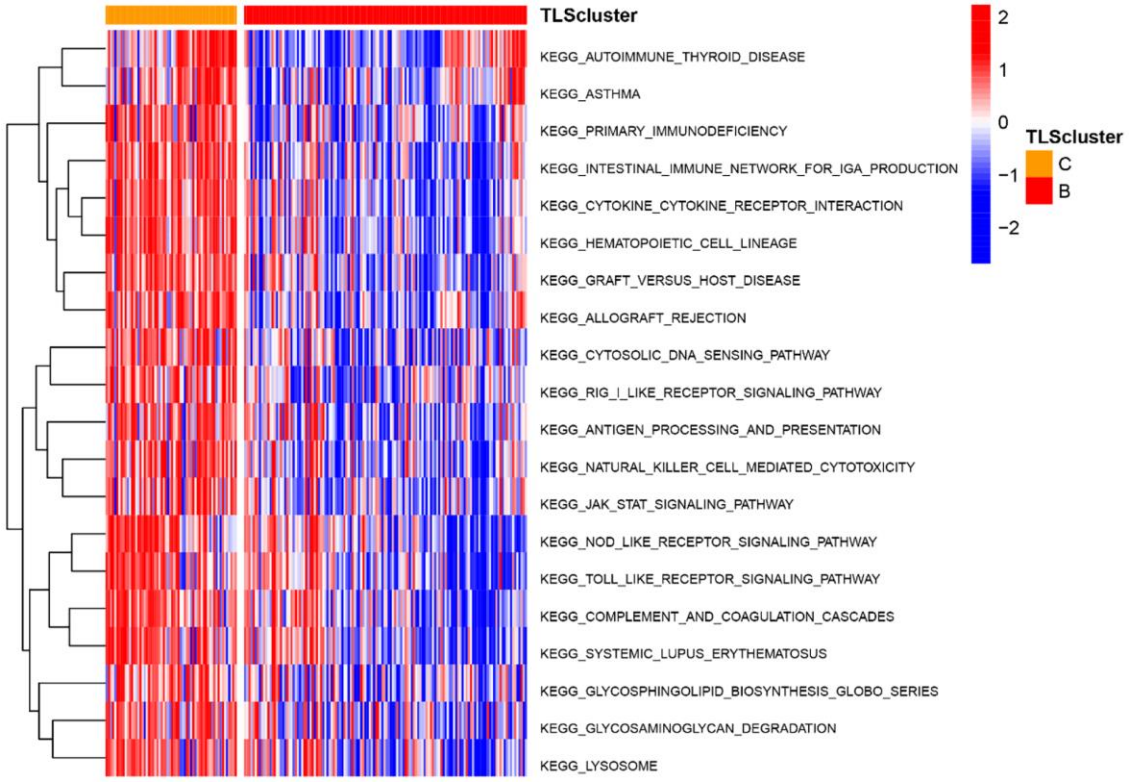

Supplementary Figure 13. The top 20 potential biological functions between subtype B and C in GSE16011.

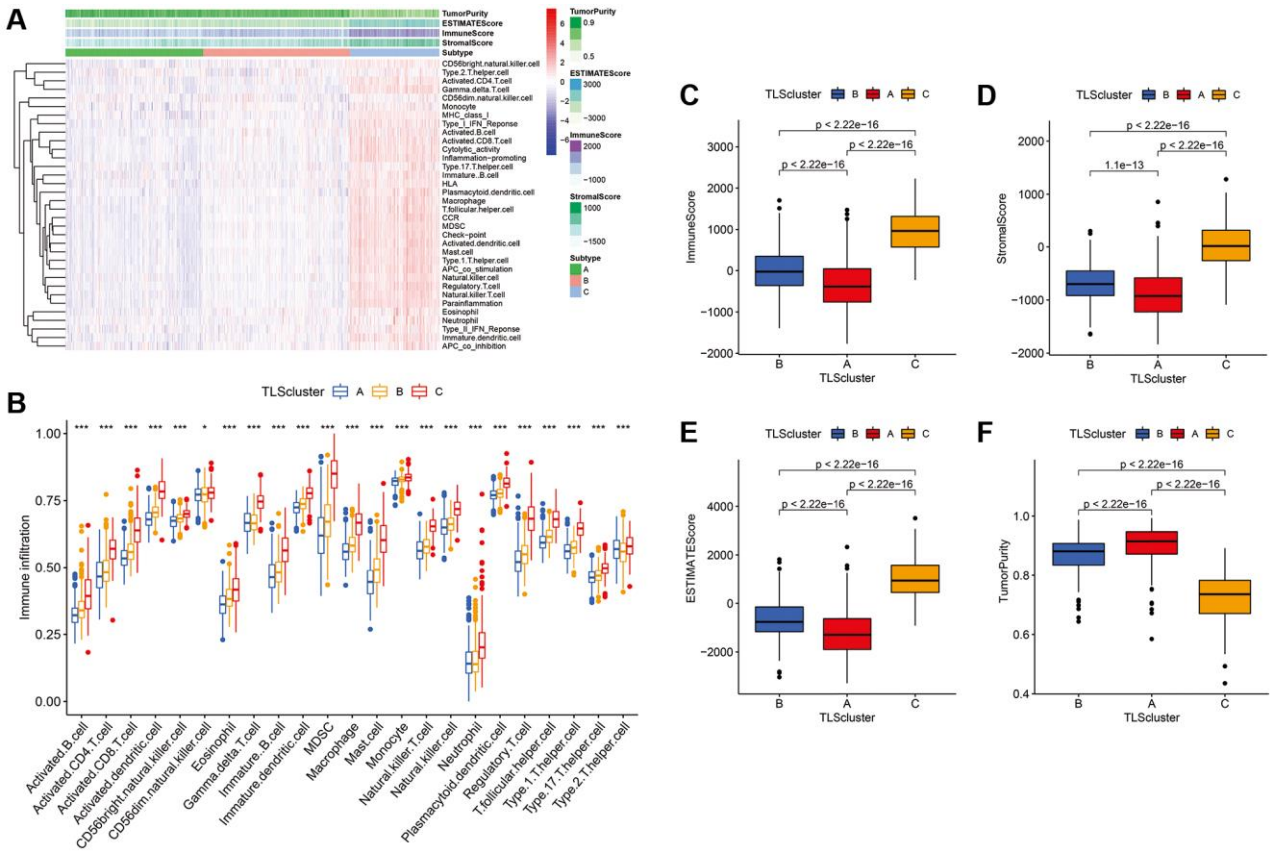

Supplementary Figure 14. Immune infiltration and tumor microenvironment of three metabolic subtypes in CGGA_cohort1. (**A**) Heatmap of TLS subtypes associated with immune infiltration and immune function. (**B**) The signature of 23 immune cell among TLS subtypes. (**C**–**F**) tumor microenvironment of TLS subtypes. C subtype had higher immune, stromal, and ESTIMATE scores compared with the scores of the A and B subtypes; however, tumor purity was lower.

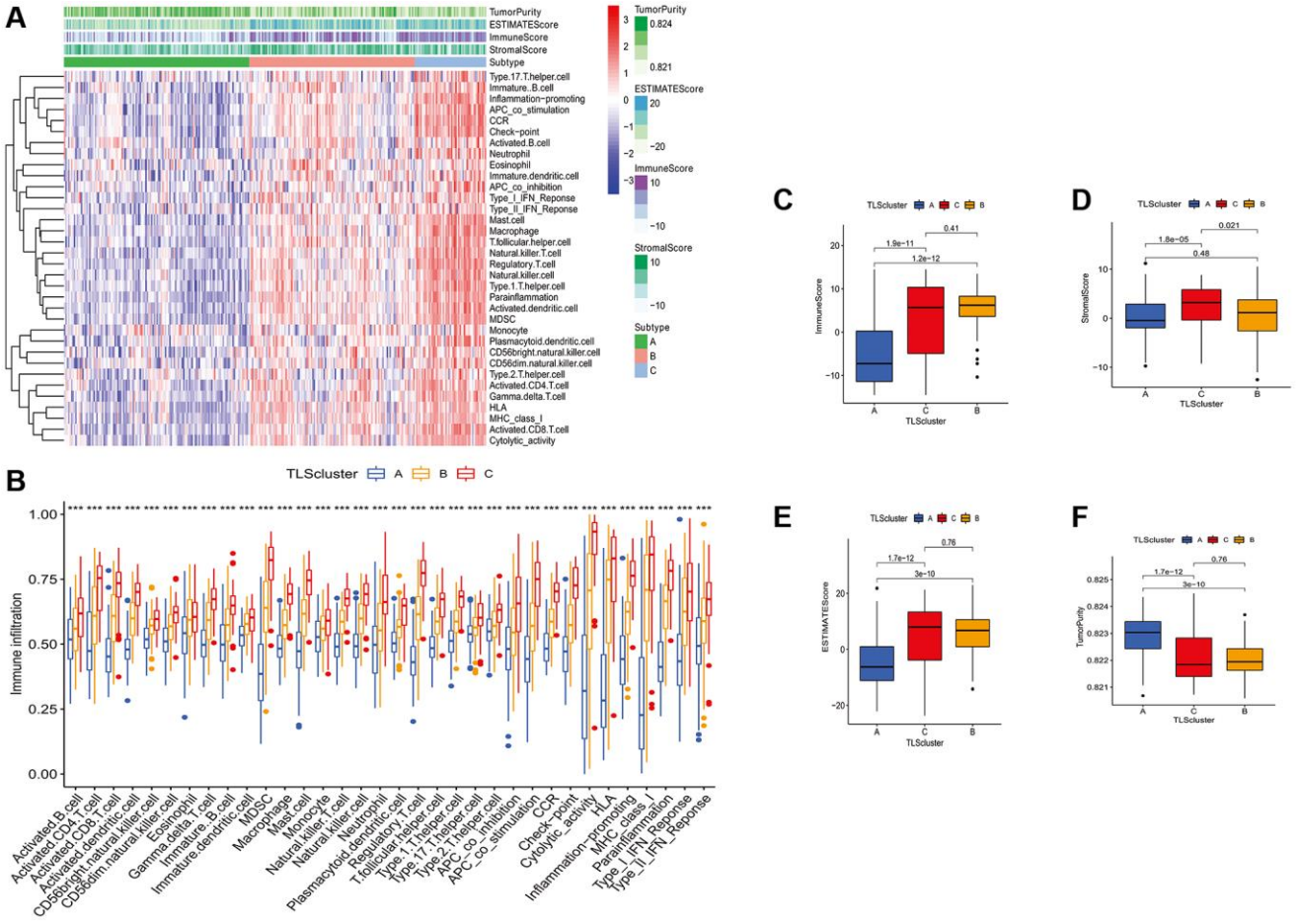

Supplementary Figure 15. Immune infiltration and tumor microenvironment of three metabolic subtypes in CGGA_cohort2. (**A**) Heatmap of TLS subtypes associated with immune infiltration and immune function. (**B**) The signature of 23 immune cell among TLS subtypes. (**C**–**F**) tumor microenvironment of TLS subtypes. C subtype had higher immune, stromal, and ESTIMATE scores compared with the scores of the A and B subtypes; however, tumor purity was lower.

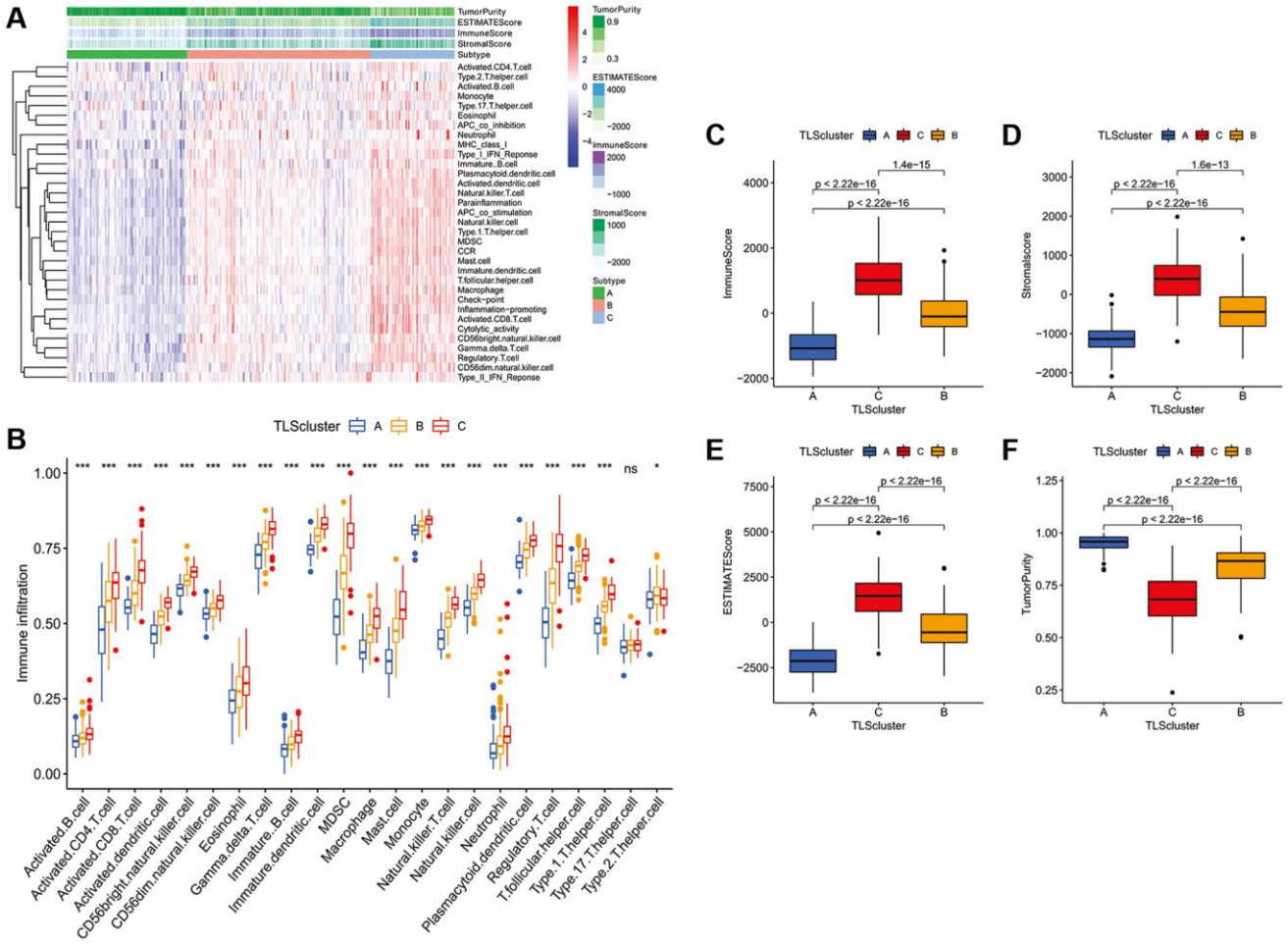

Supplementary Figure 16. Immune infiltration and tumor microenvironment of three metabolic subtypes in GSE16011. (**A**) Heatmap of TLS subtypes associated with immune infiltration and immune function. (**B**) The signature of 23 immune cell among TLS subtypes. (**C**–**F**) tumor microenvironment of TLS subtypes. C subtype had higher immune, stromal, and ESTIMATE scores compared with the scores of the A and B subtypes; however, tumor purity was lower.

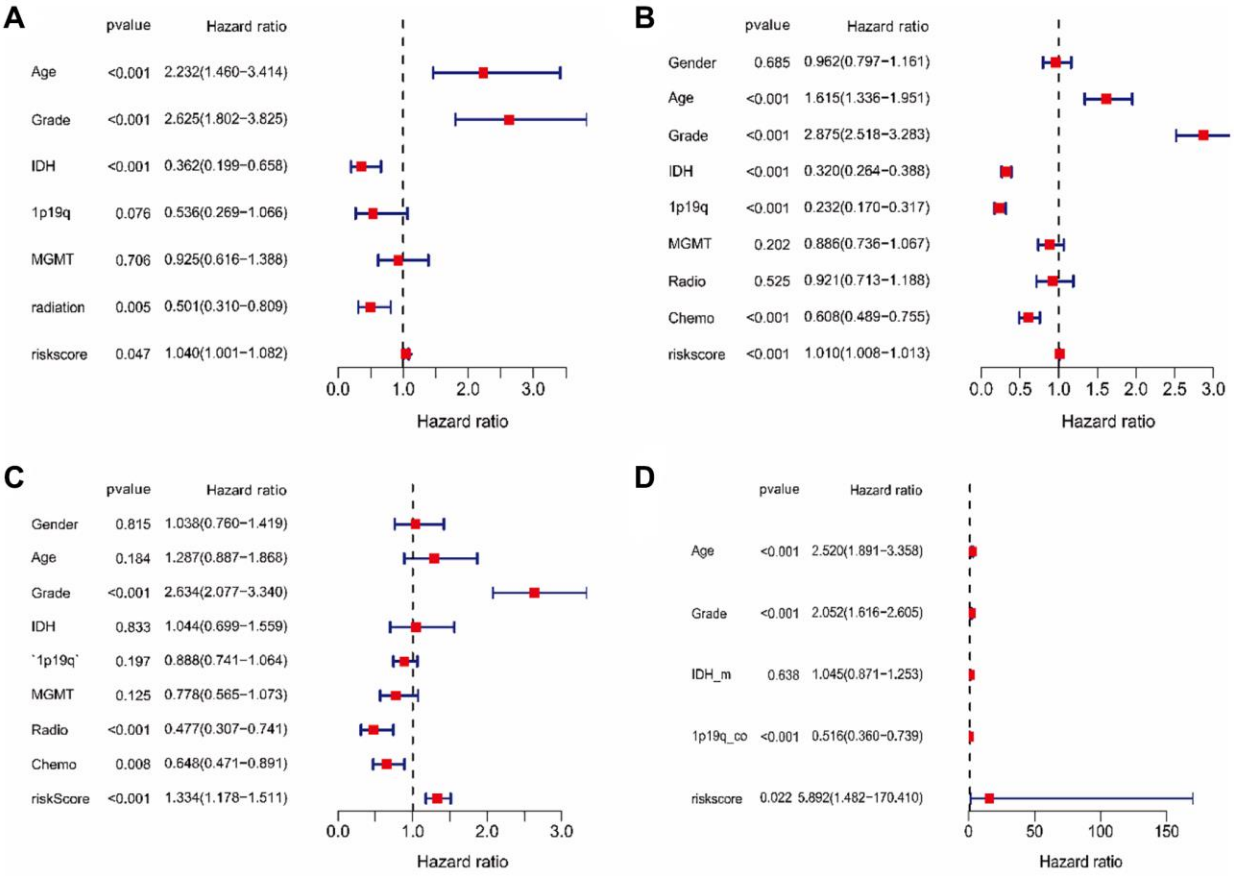

Supplementary Figure 17. Multivariate Cox regression analysis of riskscore in TCGA cohort (**A**), CGGA_cohort1 (**B**), CGGA_cohort2 (**C**) and GSE16011 (**D**).

Supplementary Tables

Supplementary Table 1. IGP was estimated for each TLS subtype in three CGGA_cohort1, CGGA_cohort2, and GSE16011.

TLS subtypes	CGGA_cohort1	CGGA_cohort2	GSE16011
A	0.943	0.921	0.933
B	0.865	0.831	0.81
C	0.789	0.709	0.701

Supplementary Table 2. Clinical characteristics of patients with distinct TLS subtypes in TCGA cohort.

Variables	TLS cluster			*p* value
	A	B	C	
Age(Year)				<0.001
≥55	29	61	70	
<55	165	131	53	
Histology				<0.001
A	29	15	2	
AA	39	35	23	
AO	25	43	7	
AOA	12	17	8	
GBM	1	31	81	
O	88	35	0	
OA	22	16	2	
Grade				<0.001
WHO II	114	67	4	
WHO III	79	94	38	
WHO IV	1	31	81	
IDH				
Mutation	187	126	24	
Wildtype	7	66	99	
1p19				<0.001
Codeletion	67	64	3	
Noncodeletion	127	128	120	
MGMT				<0.001
Methylated	172	148	64	
Unmethylated	22	44	59	
Radiotherapy				<0.001
Yes	102	143	99	
No	92	49	24	
Status				<0.001
Live	174	139	61	
Dead	20	53	62	

Supplementary Table 3. Clinical characteristics of patients with distinct TLS subtypes in CGGA_cohort1.

Variables	TLS cluster			*p* value
	A	B	C	
Age (Year)				
≥55	61	42	77	
<55	312	356	164	
Gender				0.424
Male	211	236	149	
Female	162	162	92	
Histology				<0.001
A	45	43	14	
AA	29	39	25	
AO	29	27	7	
AOA	70	90	18	
GBM	117	102	169	
O	33	23	0	
OA	50	74	8	
Grade				<0.001
WHO II	128	140	22	
WHO III	128	156	50	
WHO IV	117	102	169	
IDH				<0.001
Mutation	213	265	51	
Wildtype	143	103	186	
NA	17	30	4	
1p19				<0.001
Codeletion	98	110	3	
Noncodeletion	209	282	236	
NA	66	6	2	
MGMT				0.015
Methylated	191	186	96	
Unmethylated	120	144	109	
NA	62	68	40	
Radiotherapy				<0.001
Yes	280	297	188	
No	65	68	28	
NA	28	33	25	
Chemotherapy				<0.001
Yes	228	235	169	
No	105	123	45	
NA	40	40	27	
Status				<0.001
Live	167	182	48	
Dead	176	190	169	
NA	30	26	24	

Supplementary Table 4. Clinical characteristics of patients with distinct TLS subtypes in CGGA_cohort2.

Variables	TLS cluster			*p* value
	A	B	C	
Age (Year)				0.009
≥55	20	16	16	
<55	112	101	33	
Gender				0.183
Male	72	71	34	
Female	60	46	15	
Histology				<0.001
A	37	41	2	
AA	19	13	5	
AO	6	7	2	
AOA	3	2	0	
GBM	36	38	40	
O	20	3	0	
OA	11	3	0	
Grade				<0.001
WHO II	68	47	2	
WHO III	28	22	7	
WHO IV	2	7	40	
IDH				<0.001
Mutation	77	51	6	
Wildtype	54	66	42	
NA	1	0	1	
1p19				<0.001
Codeletion	13	2	1	
Noncodeletion	33	20	23	
NA	86	95	25	
MGMT				0.04
Methylated	53	29	16	
Unmethylated	71	81	33	
NA	8	7	0	
Radiotherapy				0.012
Yes	105	97	3	
No	21	17	7	
NA	6	3	8	
Chemotherapy				0.163
Yes	56	55	21	
No	64	58	21	
NA	12	4	7	
Status				0.016
Live	54	39	7	
Dead	71	73	40	
NA	7	40	2	

Supplementary Table 5. Clinical characteristics of patients with distinct TLS subtypes in GSE16011.

Variables	TLS cluster			
	A	B	C	*p* value
Age (Year)				0.001
≥55	20	51	34	
<55	60	80	26	
Grade				<0.001
WHO I	2	4	1	
WHO II	15	8	1	
WHO III	36	39	10	
WHO IV	27	80	48	
IDH				0.007
Mutation	34	35	12	
Wildtype	28	68	39	
NA	18	28	9	
Status				0.884
Live	10	16	6	
Dead	70	115	54	

Please browse Full Text version to see the data of Supplementary Table 6.

Supplementary Table 6. Association of TLS subtype and drug sensitivity.

Supplementary Table 7. The genes used to define the immune cell population.

Immune cell	Gene										
Activated.B.cell	ADAM28	CD180	CD79B	BLK	CD19	MS4A1	TNFRSF17	IGHM	GNG7	MICAL3	SPIB
	HLA-DOB	IGKC	PNOC	FCRL2	BACH2	CR2	TCL1A	AKNA	ARHGAP25	CCL21	CD27
	CD38	CLEC17A	CLEC9A	CLECL1							
Activated.CD4.T.cell	AIM2	BIRC3	BRIP1	CCL20	CCL4	CCL5	CCNB1	CCR7	DUSP2	ESCO2	
	ETS1	EXO1	EXOC6	IARS	ITK	KIF11	KNTC1	NUF2	PRC1	PSAT1	RGS1
	RTKN2	SAMSN1	SELL	TRAT1							
Activated.CD8.T.cell	ADRM1	AHSA1	C1GALT1C1	CCT6B	CD37	CD3D	CD3E	CD3G	CD69	CD8A	CETN3
	GPT2	GZMA	GZMH	GZMK	IL2RB	LCK	MPZL1	NKG7	PIK3IP1	PTRH2	TIMM13
	CSE1L	GEMIN6	GNLY	ZAP70							
Activated.dendritic.cell	ABCD1	C1QC	CAPG	CCL3L3	CD207	CD302	ATP5B	ATP5L	ATP6V1A	BCL2L1	C1QB
	SNURF	SPCS3	CCNA1	CEACAM8	NOS2	SRA1	TNFRSF6B	TREM1	TREML1	RHOA	SLC25A37
	TNFSF14	TREML4	VNN2	XPO6	CLEC4C	TNFAIP2	UBD	ACTR3	RAB1A	SLA	HLA-DQA2
	SIGLEC5	SLAMF9									
CD56bright.natural.killer.cell	ABAT	C11orf75	C5orf15	CDHR1	DCAF12	DYNLL1	GPR137B	HCP5	HDGFRP2	KRT86	MLST8
	ELMOD3	ENTPD5	FAM119A	FAM179A	CLIC2	COX7A2L	CREB3L4	CSF1	CSNK2A2	CSTA	CSTB
	CTPS	CTSD	FST	GATA2	GMPR	HDC	HEY1	HOXA1	HS2ST1	HS3ST1	BCL11B
CD56dim.natural.killer.cell	CDH3	MYL6B	NAA16	ClQA	ClQB	CYP27B1	EIF3M				
	CYP27A1	DDX55	DYRK2	RPL37A	NOTCH3	AKR7A3	GPRC5C	GRIN1	HLA-E	PORCN	PSMC4
	UPP1	IL21R	KIR2DS1	KIR2DS2	KIR2DS5						
Eosinophil	GIPR	KRT18P50	LRMP	FOSB	RRP12	GPR183	NR4A3	ST3GAL6	DEPDC5	PDE6C	PKD2L2
	GPR65	IL5RA	P2RY14	DACH1	DAPK2	EMR3					
Gamma.delta.T.cell	ACP5	AQP9	BTN3A2	C1orf54	CARD8	CCL18	CD209	CD33	CD36	CDK5	IL10RB
	KLRF1	LGALS1	MAPK7	KLHL7	KRT80	LAMC1	LCORL	LMNB1	MEIS3P1	MPL	FABP1
	FABP5	FADD	MFAP3L	MINPP1	RPS24	RPS7	RPS9	DBNL	CCL13		
Immature..B.cell	CD22	CYBB	FAM129C	FCRL1	FCRL3	FCRL5	FCRLA	HDAC9	HLA-DQA1	HVCN1	KIAA0226
	NCF1	NCF1B	P2RY10	SP100	TXNIP	STAP1	TAGAP	ZCCHC2			
Immature.dendritic.cell	ACADM	AHCYL1	ALDH1A2	ALDH3A2	ALDH9A1	ALOX15	AMT	ARL1	ATIC	ATP5A1	CAPZA1
	LILRA5	RDX	RRAGD	TACSTD2	INPP5F	RAB38	PLAU	CSF3R	SLC18A2	AMPD2	CLTB
	C1orf162										
MDSC	CCR2	CD14	CD2	CD86	CXCR4	FCGR2A	FCGR2B	FCGR3A	FERMT3	GPSM3	IL18BP
	IL4R	ITGAL	ITGAM	PARVG	PSAP	PTGER2	PTGES2	S100A8	S100A9		
Macrophage	AIF1	CCL1	CCL14	CCL23	CCL26	CD300LB	CNR1	CNR2	EIF1	EIF4A1	FPR1
	FPR2	FRAT2	GPR27	GPR77	RNASE2	MS4A2	BASP1	IGSF6	HK3	VNN1	FES
	NPL	FZD2	FAM198B	HNMT	SLC15A3	CD4	TXNDC3	FRMD4A	CRYBB1	HRH1	WNT5B
Mast.cell	ADAMTS3	CPA3	CMA1	CTSG	ARHGAP15	CPM	FCN1	FTL	HSPA6	ITGA9	RNASE3
	S100A4	SIGLEC8	SLC6A4	PTGS2	EGR3	PILRA					
Monocyte	ASGR2	CFP	ASGR1	CD1D	UPK3A	ACTG1	ANXA5	ATP6V1B2	CFL1	DAZAP2	CTBS
	EMR4P	HIVEP2	MARCKSL1	MBP	MMP15	PNPLA6	TMBIM6	PQBP1	TEX264	IKZF1	
Natural.killer.T.cell	BTN2A2	CD101	CD109	CNPY3	CNPY4	CREB1	CRTC2	CRTC3	CSF2	KLRC1	FUT4
	ICAM2	IL32	LAMP2	LILRB5	KLRG1	HSPA4	HSPB6	ISM2	ITIH2	KDM4C	KIR2DS4
	KIRREL3	SDCBP	NFATC2IP	MICB	KIR2DL1	KIR2DL3	KIR3DL1	KIR3DL2	NCR1	FOSL1	TSLP
Natural.killer.cell	SLC7A7	SPP1	TREM2	UBASH3A	YBX2	CCDC88A	CLEC1A	THBD	PDPN	VCAM1	EMR1
	AKT3	AXL	BST2	CDH2	CRTAM	CSF2RA	CTSZ	CXCL1	CYTH1	DAXX	DGKH
	DLL4	DPYD	ERBB3	F11R	FAM27A	FAM49A	FASLG	FCGR1A	FN1	FSTL1	FUCA1
	GBP3	GLS2	GRB2	LST1	BCL2	CDC5L	FGF18	FUT5	FZR1	GAGE2	IGFBP5
	KANK2	LDB3									

Neutrophil	CREB5	CDA	CHST15	S100A12	APOBEC3A	CASP5	MMP25	HAL	C1orf183	FFAR2	MAK
	CXCR1	STEAP4	MGAM	BTNL8	CXCR2	TNFRSF10C	VNN3				
Plasmacytoid.dendritic.cell	CBX6	DAB2	DDX17	HIGD1A	IDH3A	IL3RA	MAGED1	NUCB2	OFD1	OGT	PDIA4
	SERTAD2	SIRPA	TMED2	ENG	FCAR	IGF1	ITGA2B	GABARAP	GPX1	KRT23	PROK2
	RALB	RETNLB	RNF141	SEC14L1	SEPX1	EMP3	CD300LF	ABTB1	KLHL21	PHRF1	
Regulatory.T.cell	CCL3L1	CD72	CLEC5A	FOXP3	ITGA4	L1CAM	LIPA	LRP1	LRRC42	MARCO	MMP12
	MNDA	MRC1	MS4A6A	PELO	PLEK	PRSS23	PTGIR	ST8SIA4	STAB1		
T.follicular.helper.cell	B3GAT1	CDK5R1	PDCD1	BCL6	CD200	CD83	CD84	FGF2	GPR18	CEBPA	CECR1
	CLEC10A	CLEC4A	CSF1R	CTSS	DMN	DPP4	LRRC32	MC5R	MICA	NCAM1	NCR2
	NRP1	PDCD1LG2	PDCD6	PRDX1	RAE1	RAET1E	SIGLEC7	SIGLEC9	TYRO3	CHST12	CLIC3
	IVNS1ABP	KIR2DL2	LGMN								
Type.1.T.helper.cell	CD70	TBX21	ADAM8	AHCYL2	ALCAM	B3GALNT1	BBS12	BST1	CD151	CD47	CD48
	CD52	CD53	CD59	CD6	CD68	CD7	CD96	CFHR3	CHRM3	CLEC7A	COL23A1
	COL4A4	COL5A3	DAB1	DLEU7	DOC2B	EMP1	F12	FURIN	GAB3	GATM	GFPT2
	GPR25	GREM2	HAVCR1	HSD11B1	HUNK	IGF2	RCSD1	RYR1	SAV1	SELE	SELP
	SH3KBP1	SIT1	SLC35B3	SIGLEC10	SKAP1	THUMPD2	TIGIT	ZEB2	ENC1	FAM134B	FBXO30
	FCGR2C	STAC	LTC4S	MAN1B1	MDH1	MMD	RGS16	IL12A	P2RX5	CD97	ITGB4
	ICAM3	METRNL	TNFRSF1A	IRF1	HTR2B	CALD1	MOCOS	TRAF3IP2	TLR8	TRAF1	DUSP14
Type.17.T.helper.cell	IL17A	IL17RA	C2CD4A	C2CD4B	CA2	CCDC65	CEACAM3	IL17C	IL17F	IL17RC	IL17RE
	IL23A	ILDR1	LONRF3	SH2D6	TNIP2	ABCA1	ABCB1	ADAMTS12	ANK1	ANKRD22	B3GALT2
	CAMTA1	CCR9	CD40	GPR44	IFT80						
Type.2.T.helper.cell	ASB2	CSRP2	DAPK1	DLC1	DNAJC12	DUSP6	GNAI1	LAMP3	NRP2	OSBPL1A	PDE4B
	PHLDA1	PLA2G4A	RAB27B	RBMS3	RNF125	TMPRSS3	GATA3	BIRC5	CDC25C	CDC7	CENPF
	CXCR6	DHFR	EVI5	GSTA4	HELLS	IL26	LAIR2				